UNIVERSIDADE FEDERAL DE MINAS GERAIS
ESCOLA DE ENGENHARIA
PROGRAMA DE PÓS-GRADUAÇÃO EM ENGENHARIA QUÍMICA

Bruno Scalia Carneiro Ferreira Leite

Simulation and optimization of styrene reactors: evolutionary and gradient-based approaches

BELO HORIZONTE – MG
2022

Bruno Scalia Carneiro Ferreira Leite

Simulation and optimization of styrene reactors: evolutionary and gradient-based approaches

Dissertação apresentada ao Programa de Pós-Graduação em Engenharia Química da Escola de Engenharia da Universidade Federal de Minas Gerais, como requisito parcial para obtenção do Grau de Mestre em Engenharia Química.

Linha de Pesquisa: Engenharia de sistemas em processos.

Orientador: Esly Ferreira da Costa Junior.

BELO HORIZONTE – MG
2022

Leite, Bruno Scalia Carneiro Ferreira.
L533s Simulation and optimization of styrene reactors [recurso eletrônico] : evolutionary and gradient-based approaches / Bruno Scalia Carneiro Ferreira Leite. - 2022.
1 recurso online (106 f. : il., color.) : pdf.

Orientador: Esly Ferreira da Costa Junior.

Dissertação (mestrado) - Universidade Federal de Minas Gerais, Escola de Engenharia.

Apêndices: f. 98-106.

Bibliografia: f. 91-97.
Exigências do sistema: Adobe Acrobat Reader.

1. Engenharia química - Teses. 2. Algoritmos evolutivos - Teses. 3. Estireno - Teses. 4. Otimização multiobjetivo - Teses. 5. Reatores - Cálculo - Teses. I. Costa Junior, Esly Ferreira da. II. Universidade Federal de Minas Gerais. Escola de Engenharia. III. Título.

CDU: 66.0(043)

Ficha catalográfica elaborada pelo Bibliotecário Reginaldo César Vital dos Santos CRB/6 2165
Biblioteca Prof. Mário Werneck, Escola de Engenharia da UFMG

UNIVERSIDADE FEDERAL DE MINAS GERAIS
ESCOLA DE ENGENHARIA
PROGRAMA DE PÓS-GRADUAÇÃO EM ENGENHARIA QUÍMICA

FOLHA DE APROVAÇÃO

"SIMULATION AND OPTIMIZATION OF STYRENE REACTORS: EVOLUTIONARY AND GRADIENT-BASED APPROACHES"

Bruno Scalia Carneiro Ferreira Leite

Dissertação submetida à Banca Examinadora designada pelo Colegiado do Programa de Pós-Graduação em Engenharia Química da Escola de Engenharia da Universidade Federal de Minas Gerais, como parte dos requisitos à obtenção do título de **MESTRE EM ENGENHARIA QUÍMICA**.

298ª DISSERTAÇÃO APROVADA EM 9 DE DEZEMBRO DE 2022 POR:

Documento assinado eletronicamente por **Esly Ferreira da Costa Junior, Professor do Magistério Superior**, em 09/12/2022, às 11:21, conforme horário oficial de Brasília, com fundamento no art. 5º do Decreto nº 10.543, de 13 de novembro de 2020.

Documento assinado eletronicamente por **Andrea Oliveira Souza da Costa, Coordenador(a) de curso de pós-graduação**, em 09/12/2022, às 11:22, conforme horário oficial de Brasília, com fundamento no art. 5º do Decreto nº 10.543, de 13 de novembro de 2020.

Documento assinado eletronicamente por **Eder Domingos de Oliveira, Professor do Magistério Superior**, em 09/12/2022, às 11:23, conforme horário oficial de Brasília, com fundamento no art. 5º do Decreto nº 10.543, de 13 de novembro de 2020.

A autenticidade deste documento pode ser conferida no site https://sei.ufmg.br/sei/controlador_externo.php?acao=documento_conferir&id_orgao_acesso_externo=0, informando o código verificador **1908880** e o código CRC **FE15DDCB**.

Referência: Processo nº 23072.268245/2022-16 SEI nº 1908880

To my late grandparents

ACKNOWLEDGEMENTS

I was unprepared to face the challenges of these last few years. In fact, I could not imagine their extent or what I would be able to achieve. If I know something, it is that, if not for the support I had in this journey, I would be somewhere else, but today I do not want to imagine myself anywhere else but here. This is to Prof. Esly F. da Costa Junior.

To the amazing professors I met during my time in the Chemical Engineering Department, I express my most sincere gratitude. Although not the only ones, I would like to thank Prof. Julio Cézar Balarini, Prof. Andréa O. S. da Costa, and Prof. Éder D. de Oliveira for introducing me to amazing problems and supporting me throughout them.

To the ones who raised me and helped me to become who I am today, whom I call “family”, blood relatives or not, my most sincere gratitude.

To my dearest friends and family, for their emotional support in these recent overwhelming years, my deepest thanks.

I thank whatever gods may be; For my unconquerable soul – William Ernest Henley

ABSTRACT

Styrene (ST) is one of the most important monomers produced by the chemical industry, used as a feedstock in a variety of polymer products. Direct dehydrogenation of ethylbenzene (EB) to styrene is the most usual alternative for commercial production, a process in which the reactor is considered the most critical equipment. Therefore, efforts are directed towards enhancing its efficiency, in which simulation and numerical optimization are relevant routes. In this work, steady-state adiabatic axial-flow and radial-flow catalyst dehydrogenation reactors were simulated based on an intrinsic realistic heterogeneous kinetic model, which would adequately encompass the complex influence of the decision variables in the system. Once the results were validated, two routes for optimizing performance were explored: gradient-based optimization and multi-objective evolutionary algorithms. In the first approach, axial and radial-flow designs were compared and the impact of operating temperatures, catalyst loading, and pressure on reactor performance was investigated. In the second approach, the analysis was extended to the impact of steam-to-ethylbenzene feed ratio, which is a relevant heat consumer in the process, and the number of catalyst beds, besides an additional analysis of the decision variables aforementioned. Several optimal scenarios were obtained, which can be used in an integrated process analysis to define suitable operational conditions according to the specific context of industrial units. Furthermore, the contribution of the current study includes making the DE algorithms, orthogonal collocation, and reactor simulation implemented code available in public code repositories and Python packages.

Keywords: Multi-objective optimization; Evolutionary algorithms; Differential Evolution; Styrene; Reaction engineering.

RESUMO

O estireno (ST) é um dos monômeros mais importantes produzidos pela indústria química, utilizado como matéria-prima em uma variedade de polímeros. A desidrogenação direta do etilbenzeno (EB) em estireno é a alternativa mais usual para a produção comercial, processo no qual o reator é considerado o equipamento mais crítico. Portanto, os esforços são direcionados para aumentar sua eficiência, na qual a simulação e a otimização numérica desempenham um papel importante. Neste trabalho, reatores adiabáticos de desidrogenação catalítica de fluxo axial e radial em estado estacionário foram simulados com base em um modelo cinético heterogêneo intrínseco realista, que abrange adequadamente a complexa influência de variáveis de decisão do sistema. Uma vez validados os resultados, dois caminhos para otimizar o desempenho foram explorados: otimização convexa utilizando algoritmos baseados em gradiente e algoritmos evolucionários multiobjetivo. Na primeira abordagem, os projetos de fluxo axial e radial foram comparados e o impacto das temperaturas de operação, carga do catalisador e pressão no desempenho do reator foi investigado. Na segunda abordagem, a análise foi estendida para o impacto da razão de alimentação entre vapor e etilbenzeno, que é um consumidor de calor relevante no processo, como também para o número de leitos de catalisadores, além de uma análise adicional das variáveis de decisão já mencionadas. Foram obtidos diversos cenários ótimos, que podem ser utilizados em uma análise integrada de processos para definir condições operacionais adequadas de acordo com o contexto específico das unidades industriais. Além disso, a contribuição do presente estudo inclui disponibilizar os algoritmos de otimização implementados, o código de colocação ortogonal e de simulação de reatores em repositórios públicos de código e pacotes Python.

Palavras-chave: Otimização multi-objetivo; Algoritmos evolucionários; Evolução diferencial; Estireno; Cálculo de reatores.

LIST OF FIGURES

LIST OF TABLES

ABBREVIATIONS

BZ	Benzene
DE	Differential Evolution
EA	Evolutionary algorithm
EB	Ethylbenzene
GDE3	Generalized Differential Evolution 3
MOEA	Multi-objective evolutionary algorithm
MOO	Multi-objective optimization
NSDE	Nondominated Sorting Differential Evolution
NSGA-II	Nondominated Sorting Genetic Algorithm II
SLSQP	Sequential Least-Squares Programming
SOO	Single-objective optimization
ST	Styrene
TO	Toluene

SYMBOLS

A	pre-exponential factor of the Arrhenius equation, kmol/(m³ h bar), kmol/(kg_{cat}·h), bar^{-1}
A_c	cross-sectional area of the reactor bed, m²
C_{pi}	specific heat for each component *i*, kJ/(kmol·K)
CR	crossover parameter in differential evolution, -
$D_{e,j}$	effective molecular diffusion coefficient of the component *j*, m²/s
D_{jk}	binary molecular diffusion coefficient for component *j* in component *k*, m²/s
D_{jm}	molecular diffusion coefficient for component *j* in the gas mixture, m²/s
dp	pellet diameter, m
$\dot{E}_{gen}$	Energy generation rate, kJ/h
F	mutation parameter of differential evolution; molar flow rate, kmol/h
f	objective function, -
f_{ws}	objective function of weighted sum subproblem, -
G	superficial mass flow, kg/(m²·s),
K_{eq}	equilibrium coefficient, -
K	adsorption coefficient, bar^{-1}
N	number of individuals, -
P_j	partial pressure of component *j*, bar
$P_{s,j}$	partial pressure of component *j* inside the catalyst, bar
r	pellet radial coordinate, m
r_{ci}	rate of catalytic equation *i*, kmol/(kg_{cat}·h)
r_{cij}	rate of generation of component *j* in catalytic equation *i*, kmol/(kg_{cat}·h)
R_g	ideal gases constant, m³·bar/(kmol·K)
r_j	rate of generation of the component *j*, kmol/(m³·h)
r_s	value of the pellet radius on its surface, m
r_{ti}	rate of thermal equation *i*, kmol/(m³·bar·h)
r_{tij}	rate of generation of component *j* in thermal equation *i*, kmol/(m³·bar·h)

S_{ST}	styrene selectivity, %
T	temperature, K
T_R	reduced temperature, K
$\boldsymbol{u}$	new trial vector in differential evolution, -
$\boldsymbol{v}$	new mutant vector in differential evolution, -
W	catalyst bed mass (loading), kg
w	weight of objective function, -
$\boldsymbol{x}_r$	parent vector randomly selected in differential evolution, -
X_{ST}	styrene conversion, %
y	molar fraction, -
ΔG^0	standard Gibbs energy change, kJ/kmol
ΔH_a	adsorption enthalpy change, kJ/mol
ΔH_f	heat of formation, kJ/kmol
ΔH_r	heat of reaction, kJ/kmol
ΔS^0	standard entropy change, kJ/(kmol·K)

Greek letters

γ	jitter deviation parameter, -
εb	bulk void fraction of the catalyst bed, -
εs	void fraction inside the catalyst, -
η	effectiveness factor of the catalytic reaction i, -
μ	gas viscosity in kg/(m·s)
μ_i	viscosity of component i in the gas mixture, μP
ρ_b	bulk density of the catalyst bed, kg/m³
ρ_{gas}	gas density kg/m³
ρ_s	catalyst solid density in kg/m³
τ	tortuosity factor, -

SUMMARY

1. INTRODUCTION

Styrene (ST) is one of the most important monomers produced by the chemical industry today (Chevron Phillips Chemical, 2021). It is used as a feedstock in a variety of polymer products: thermoplastics, elastomers, dispersions, and thermoset plastics (James & Castor, 2011). Its annual production is over 30 million tonnes per year (Business Wire, 2021) and a steady increase is expected in the next years, mainly in the part of the world knowing rapid development, such as China and Southern Asia (Dimian, et al., 2019).

The industry is capital-intensive and characterized by economies of scale. Industrial units with a capacity of over 600,000 tonnes of ST per year have been reported (Focus on Surfactants, 2020; ENI-Versalis, s.d.). This reinforces the impact of economic returns by process improvements, as in the present competitive styrene market even small differences in raw materials and utility consumption can heavily influence profit (ENI-Versalis, s.d.).

Direct dehydrogenation of ethylbenzene (EB) to styrene accounts for 85% of commercial production. The reaction is carried out in the vapor phase with steam over a catalyst consisting primarily of iron oxide. The reaction is endothermic and can be accomplished either adiabatically or isothermally. Both methods are used in practice (James & Castor, 2011). The reactor is considered the most critical equipment of the process (Yee, et al., 2003), thus efforts are directed to enhance its efficiency.

One relevant strategy for process improvement is developing new catalyst technology, which is the focus of several studies (Wang, et al., 2021; Fedotov, et al., 2021; Sancheti & Yadav, 2021). Other strategies involve reactor modeling, simulation, and optimization (Sundaram, et al., 1991; Yee, et al., 2003; Babu, et al., 2005; Tarafder, et al., 2005; Gujarathi & Babu, 2010). Improvements in reactor selectivity and conversion are particularly desirable not only for direct economic returns but for environmental, social, and governance strategies as well, through minimizing natural resource consumption, as the manufacture of styrene via ethylbenzene consumes more than 50% of the commercial benzene in the world (Chen, 2006).

Maximizing styrene conversion and selectivity are conflicting objectives, as increasing conversion increases the production of by-products, lowering

selectivity. They can be combined in a multi-objective optimization (MOO) problem. Such problems can be solved using different approaches, that are usually distinguished between two broad categories (Rangaiah, et al., 2020). The first includes strategies that transform the main problem into single-objective subproblems solved by established single-objective algorithms. Two common techniques following this approach are the weighted sum and ε-constraint techniques. Alternatively, some strategies solve the conflicting objectives simultaneously. Techniques following this approach are metaheuristics (or stochastic algorithms) that are mostly population-based and include evolutionary algorithms (Rangaiah, et al., 2020).

Evolutionary algorithms (EAs) can overcome some of the disadvantages of gradient-based optimization techniques, such as convergence dependence on to initial solution and getting stuck at suboptimal points (Deb, 2004). However, non-gradient-based evolutionary methods used to solve MOO problems can lead to large numbers of objective function evaluations (Rangaiah, et al., 2020), which can be computationally expensive. Although stochastic methods are time-consuming, they have become popular due to their applicability to any type of optimization problem, reliability in locating the global optimum, relative simplicity of algorithms, and easy adaptability for MOO (Rangaiah & Sharma, 2017).

Some of the most popular multi-objective evolutionary algorithms (MOEAs) are NSGA-II (Deb, et al., 2002), SPEA2 (Zitzler, et al., 2001), MOEA/D (Zhang & Li, 2007), and GDE3 (Kukkonen & Lampinen, 2005). Differential evolution (DE) (Storn & Price, 1997) was originally designed for scalar objective optimization. Nevertheless, because of the simple implementation and efficient problem-solving quality of DE, it is used to solve several multi-objective optimization problems (Ayaz, et al., 2020). Multi-objective differential evolution algorithms are sometimes referred to as MODE, denoting either a collection of or specific algorithms (Babu & Anbarasu, 2005; Xue, et al., 2003; Babu, et al., 2005), although implementations are usually different. Besides GDE3, some examples are PDE (Abbass, et al., 2001), DEMO (Robič & Filipič, 2005), GAMODE (Cheng, et al., 2016), NSDE (Iorio & Li, 2004), and I-MODE (Sharma & Rangaiah, 2013).

Relevant studies have explored applications of MOEAs to chemical engineering processes (Fierens, et al., 2015; Bakhshi Ani, et al., 2015; Reddy, et al., 2017; Chaudhari & Garg, 2019; Li, et al., 2020), of which some have been

directed toward the styrene reactor, each with a specific focus. Yee et al. (2003) are among the first authors to propose formulating the optimization of styrene reactors as a multi-objective problem. Their study used the first version of NSGA (Srinivas & Deb, 1994) and considered production, yield (conversion), and selectivity as objectives. Their results motivated the study proposed by Tarafder et al. (2005), in which other processes of the manufacturing line were included in the decision-making, and the improved algorithm NSGA-II (Deb, et al., 2002) was adopted. Babu et al. (2005) are among the first to apply an algorithm based on DE (MODE) to this problem, which has presented promising results compared to the genetic algorithm (GA) reproduction operator. Later, Gujarathi & Babu (2010) compared the performances of pseudo-adiabatic and steam-injected operations using MODE. Recently, Chaudhari et al. (2022) demonstrated the advantages of NSGA-III (Deb & Jain, 2014; Jain & Deb, 2014) over NSGA-II (Deb, et al., 2002) when handling more than two objectives in the same problem. However, all these studies have adopted the reaction model and reactor design proposed by Sheel & Crowe (1969), which considers catalyst technology, kinetic parameters, and industrial practice of the late 1960s and early 1970s, although significant advances have occurred in these areas, which gives a margin for revisiting the problem.

2. OBJECTIVES

2.1. GENERAL OBJECTIVE

The objective of the current study was to reproduce realistic styrene reactor simulations based on fundamental equations from literature and investigate the impact of process design aspects and operating conditions on reactor performance.

2.2. SPECIFIC OBJECTIVES

- Apply phenomena-based equations to simulate reactors of distinct configurations to compare the performances of reactors with distinct flow-patterns and design aspects.
- Apply gradient-based and evolutionary algorithms to optimize reactors in different scenarios and investigate the impact of relevant decision-making aspects on reactor performance.
- Implement and make available reproducible code for future numerical simulation and optimization.

3. LITERATURE REVIEW

3.1. INDUSTRIAL PROCESS

Styrene is commercially produced by the dehydrogenation of ethylbenzene over an iron oxide catalyst in the presence of steam. Steam is used to supply heat for this endothermic reaction and to lower the reactants' partial pressure. In addition, it protects the catalyst from coking and is applied to in situ regeneration of activity (Dimian & Bildea, 2019). Increasing the process steam that feeds the reactor helps to increase the conversion of styrene and decrease the production of undesirable byproducts. However, it increases the cost of supplying the process steam, and it increases the cost of fuel needed in the furnace to heat the steam and EB to the desired reactor inlet temperature (Luyben, 2011). Moreover, the choice of the steam-to-ethylbenzene ratio must consider its impact on the lifetime of the catalyst (Lee & Froment, 2008). According to Chen (2006), reduced downtime and increased production due to an extended catalyst lifetime are more important than savings in catalyst cost. Exergy analysis indicated that the saturated steam is responsible for the largest exergy losses which amount to 60% of the total (Ali & Hadj-Kali, 2018). Coke formation is related to catalyst deactivation by site coverage and pore blocking (Lee, 2005). Its mechanisms are precisely described by Devoldere & Froment (1999).

The dehydrogenation reaction can be accomplished either adiabatically or isothermally. Both methods are used in practice, although over 75% of all operating styrene plants carry out the dehydrogenation reaction adiabatically (James & Castor, 2011). In principle, isothermal dehydrogenation has the advantage of avoiding a very high temperature at the reactor inlet and maintaining a sufficiently high temperature at the reactor outlet. In practice, these advantages are negated by formidable heat-transfer problems (Chen, 2006).

The reactors usually contain large adiabatic beds of catalyst. Vapor flow is either downward (axial flow, Figure 1A) or radial outflow (Figure 1B). The gas flow, represented for both configurations in Figure 1, might be insightful to understanding the mathematical model presented in the following sections. Beds may be staged, with intermediate heaters or intermediate addition of hot gases

to supply the heat of reaction (McKetta Jr, 1993). Most adiabatic reactors are radial reactors (Rase, 2000). They are used for ethylbenzene dehydrogenation because their smaller pressure drops allow the reactors to operate at a lower pressure than axial-flow (Li, 2007). Since the volumetric flow increases as the reaction proceeds due to the increase in moles, the flow is directed from the inside of the annular bed radially outward (Rase, 2000).

Commercial plants typically have two or three catalyst beds in series, each contained in individual vessels, with external or internal interstage reheaters (Li, 2007). Önal, et al. (1990) studied three axial-flow adiabatic reactors in series with steam injection before each. Lee & Froment (2008) simulated a series of three catalytic beds with both axial-flow and radial-flow, the same configurations analyzed by the current study.

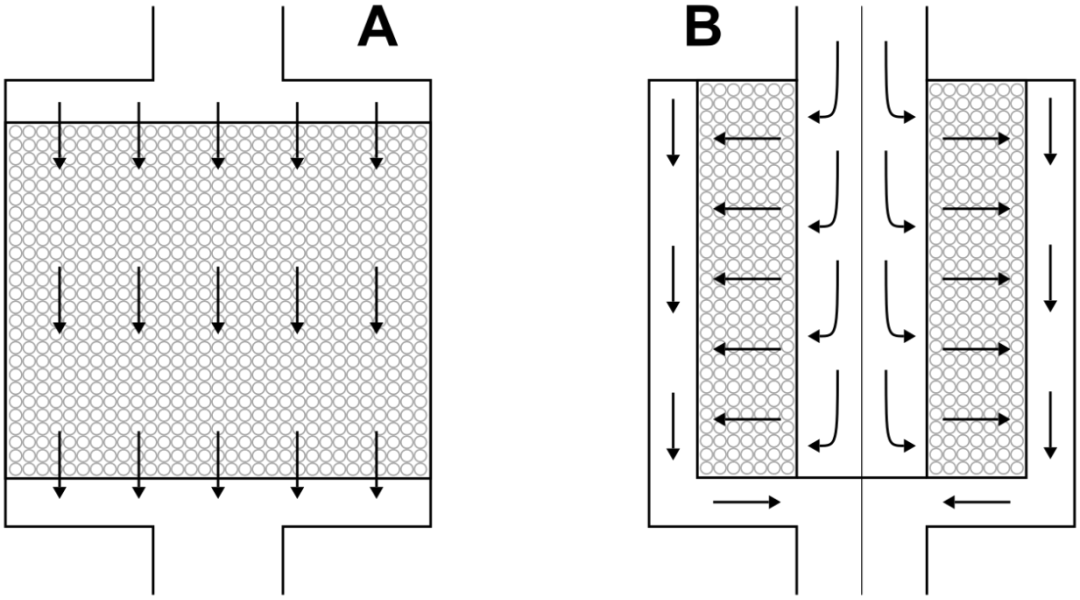

Figure 1 – Simplified cross-sectional schematic representation of gas flow in axial-flow (A) and radial-flow (B) catalytic beds.

The reactors are run at the lowest pressure that is safe and practicable. Some units operate under vacuum, while others operate at low positive pressure (James & Castor, 2011). Earlier dehydrogenation reactors were designed for operation above atmospheric pressure, at about 138 kPa (20 psia), so that a compressor would not be required to remove hydrogen from the condensed

reactor effluent. Since the 1970s, vacuum design has become standard because the benefits of high conversion and selectivity achievable and low dilution steam required at low pressure outweigh the cost of the compressor (Chen, 2006). Pressures of 41 kPa (6 psia) or lower at the reactor outlet have been designed (Chen, 2006). Nevertheless, in the current study, it was used 0.5 bar as the outlet pressure limit, following values reported by Rase (2000) for most recent reactors.

Feed temperatures are up to 640°C (Lee, 2005; James & Castor, 2011). Although higher temperatures achieved with steam addition favor the equilibrium conversion to styrene, side reactions become significant at higher reactor temperatures. The resulting high flow rates can lead to large pressure drops across tubular flow reactors (Snyder & Subramaniam, 1994).

3.2. KINETIC MODELING

The development of kinetic models is essential to be able to simulate different operational conditions proposing conceptual analysis and process improvements. Several models have been proposed over the years with different complexity levels and are suitable for distinct catalyst technology. Some models consider intraparticle diffusion and component gradients, while others do not. These approaches are usually distinguished into heterogeneous and pseudohomogeneous respectively.

Some examples of relevant pseudohomogeneous models are those proposed by Carra and Forni (1965), Sheel & Crowe (1969), and Sheppard, et al. (1986). In contrast to the pseudohomogeneous approach, Elnashaie et al. (1993) developed a rigorous heterogeneous reaction model based on the dusty gas model using effective reaction rates derived from pseudohomogeneous models. This approach was later applied by Abdalla, et al. (1994) comparing the performances of different catalysts.

Lee (2005) proposed the intrinsic heterogeneous model accounting for both catalytic and thermal reactions over a modern industrial catalyst, which was applied in the present study. The heterogeneous kinetic models have the advantage of being valid for variable catalyst pellet diameter, although they are more computationally expensive than pseudohomogeneous models. Lee (2005)

suggests that an intrinsic kinetic model would allow predicting reactor performance precisely beyond the operating range of the production unit. These results were also published by Lee & Froment (2008).

The kinetic model parameters adopted (Lee, 2005; Lee & Froment, 2008) were obtained for a high-performance catalyst (Dimian & Bildea, 2019). The results obtained using these parameters agree with values reported in industrial practice of conversion in the range between 60 to 75% and the selectivity of 85 to 95% (Rase, 2000). It corresponds to substantially superior performance and more recent technology than considered previously in optimization studies (Babu, et al., 2005; Yee, et al., 2003; Tarafder, et al., 2005; Gujarathi & Babu, 2010; Chaudhari, et al., 2022), which refer back to either the parameters of the model proposed by Sheel & Crowe (1969) or the derived parameters for the corresponding heterogeneous model proposed by Abdalla et al. (1994). Using values referring to those kinetic models, relatively poor selectivity has been reported, limiting the optimal conversion to 50 to 60% (Dimian & Bildea, 2019).

Four reactions are considered in this model: the main reaction of ethylbenzene (EB) dehydrogenation into styrene (ST) also producing H_2, and three side reactions producing benzene (BZ), ethylene (C_2H_4), toluene (TO), and methane (CH_4). A reaction scheme is presented in Figure 2.

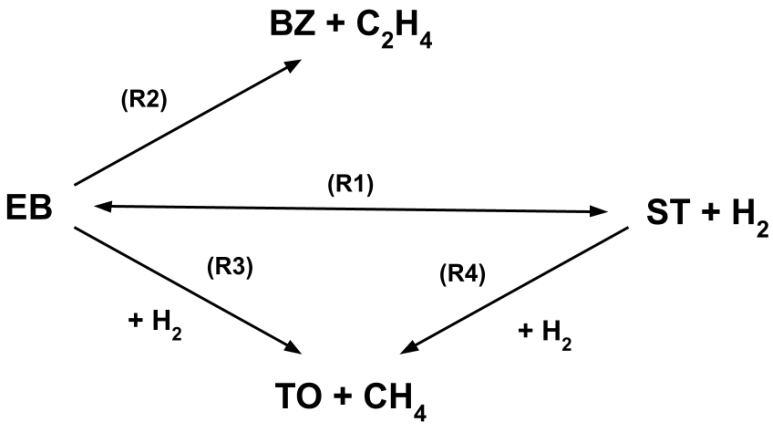

Figure 2 – Reaction scheme proposed by Lee (2005) used in this study.

$$EB \overset{k1}{\leftrightarrow} ST + H_2 \quad \text{(R1)}$$

$$EB \overset{k2}{\rightarrow} BZ + C_2H_4 \quad \text{(R2)}$$

$$EB + H_2 \overset{k3}{\rightarrow} TO + CH_4 \quad \text{(R3)}$$

$$ST + 2H_2 \overset{k4}{\rightarrow} TO + CH_4 \quad \text{(R4)}$$

The thermal reactions occur in the zones without catalyst or in the void fraction of the catalyst bed itself (Lee & Froment, 2008). They are presented in Equations 1-3 and expressed in terms of kmol/(m³·h) of EB consumed. The equilibrium coefficient K_{eq} is presented in Equation 4. The same equilibrium coefficient is considered for both thermal and catalytic reactions. Catalytic reaction rates are presented in Equations 5-8 and are expressed in terms of kmol/(kg_{cat}·h) of EB consumed, except for Equation 8 which is in terms of kmol/(kg_{cat}·h) of ST consumed. The Gibbs energy change of reaction ΔG^0 at temperature T was calculated based on values of heat capacity coefficients, standard heat of formation and standard Gibbs energy of formation of the components presented by Reid, et al. (1987). The kinetic and adsorption coefficients follow the Arrhenius equation with parameters presented in Table 1.

$$r_{t1} = k_{t1}\left(P_{EB} - \frac{P_{ST}P_{H_2}}{K_{eq}}\right) \quad (1)$$

$$r_{t2} = k_{t2}P_{EB} \quad (2)$$

$$r_{t3} = k_{t3}P_{EB} \quad (3)$$

$$K_{eq} = exp\left(\frac{-\Delta G^0}{RT}\right) \quad (4)$$

$$r_{c1} = \frac{k_{c1} K_{EB} \left(P_{EB} - \frac{P_{ST} P_{H_2}}{K_{eq}} \right)}{\left(1 + K_{EB} P_{EB} + K_{ST} P_{ST} + K_{H_2} P_{H_2} \right)^2} \quad (5)$$

$$r_{c2} = \frac{k_{c2} K_{EB} P_{EB}}{\left(1 + K_{EB} P_{EB} + K_{ST} P_{ST} + K_{H_2} P_{H_2} \right)^2} \quad (6)$$

$$r_{c3} = \frac{k_{c3} K_{EB} P_{EB} K_{H_2} P_{H_2}}{\left(1 + K_{EB} P_{EB} + K_{ST} P_{ST} + K_{H_2} P_{H_2} \right)^2} \quad (7)$$

$$r_{c4} = \frac{k_{c4} K_{ST} P_{ST} K_{H_2} P_{H_2}}{\left(1 + K_{EB} P_{EB} + K_{ST} P_{ST} + K_{H_2} P_{H_2} \right)^2} \quad (8)$$

In Equations 1-8, P_j is the partial pressure of component *j* in bar, k_{ti} is the kinetic coefficient of thermal reaction *i* in kmol/(m³·bar·h), k_{ci} is the kinetic coefficient of catalytic reaction *i* in kmol/(kg_{cat}·h), K_j is the adsorption coefficient of component *j* in bar^{-1}. The partial pressures consider ideal gas conditions by the following equation: $P_j = \frac{F_j}{F_t} P$, in which F_j is the molar flow of component *j* and F_t the total molar flow in kmol/h.

Table 1 – Kinetic parameters for reactions and adsorption (Lee & Froment, 2008).

Thermal Reactions		
Coefficient	*A* [kmol/(m³ h bar)]	*Ea* [kJ/mol]
k_{t1}	2.2215 x 10^{16}	272.23
k_{t2}	2.4217 x 10^{20}	352.79
k_{t3}	3.8224 x 10^{17}	313.06
Catalytic Reactions		
Coefficient	*A* [kmol/(kg_{cat}·h)]	*Ea* [kJ/mol]
k_{c1}	4.594 x 10^{9}	175.38
k_{c2}	1.060 x 10^{15}	296.29
k_{c3}	1.246 x 10^{26}	474.76
k_{c4}	8.024 x 10^{10}	213.78
Adsorption		
Coefficient	*A* [bar^{-1}]	$\Delta H_{a,j}$ [kJ/mol]
K_{EB}	1.014 x 10^{-5}	-102.22
K_{ST}	2.678 x 10^{-5}	-104.56
K_{H2}	4.519 x 10^{-7}	-117.95

3.3. CONTINUITY, ENERGY, AND MOMENTUM

The continuity, energy, and momentum equations were defined considering the system operating at steady-state.

The continuity equations for each component follow the basic format presented by Equation 9.

$$\frac{dF_j}{dW} = \frac{\varepsilon_b}{\rho_b}\sum_i r_{tij} + \sum_i \eta_i r_{cij} \quad (9)$$

In which, W is the catalyst mass in kg, r_{tij} is the rate of generation of component j in thermal equation i in kmol/(m³·h), r_{cij} is the rate of generation of component j in catalytic equation i in kmol/(kg_{cat}·h), η_i is the effectiveness factor of the catalytic reaction i, ρ_b is the bulk density of the catalytic bed in kg/m³, ε_b is the bulk void fraction of the catalytic bed.

For each component, are expressed by Equations 10-15.

$$\frac{dF_{EB}}{dW} = \frac{\varepsilon_b}{\rho_b}(-r_{t1} - r_{t2} - r_{t3}) + (-\eta_1 r_{c1} - \eta_2 r_{c2} - \eta_3 r_{c3}) \quad (10)$$

$$\frac{dF_{ST}}{dW} = \frac{\varepsilon_b}{\rho_b}(r_{t1}) + (\eta_1 r_{c1} - \eta_4 r_{c4}) \quad (11)$$

$$\frac{dF_{H_2}}{dW} = \frac{\varepsilon_b}{\rho_b}(r_{t1} - r_{t3}) + (\eta_1 r_{c1} - \eta_3 r_{c3} - 2\eta_4 r_{c4}) \quad (12)$$

$$\frac{dF_{BZ}}{dW} = \frac{dF_{C_2H_4}}{dW} = \frac{\varepsilon_b}{\rho_b} r_{t2} + \eta_2 r_{c2} \quad (13)$$

$$\frac{dF_{TO}}{dW} = \frac{dF_{CH_4}}{dW} = \frac{\varepsilon_b}{\rho_b} r_{t3} + (\eta_3 r_{c3} + \eta_4 r_{c4}) \quad (14)$$

$$\frac{dF_{H2O}}{dW} = 0 \quad (15)$$

The energy balance is expressed by Equation 16.

$$\frac{dT}{dW} = \frac{\sum -\Delta H_{ri}\left(\frac{\varepsilon_b}{\rho_b} r_{ti} + \eta_i r_{ci}\right)}{\sum C_{pj} F_j} \quad (16)$$

In which C_{pi} is the specific heat of component *j* in kJ/(kmol·K) and ΔH_{ri} is the heat of reaction of the reaction *i* in kJ/kmol. ΔH_{ri} was assumed to be a function of temperature only, considering ideal gases (Sandler, 1999). Values of C_{pi} and ΔH_{ri} were based calculated at each temperature based on Reid, et al. (1987).

The momentum equation expresses the pressure drop in bar/kg_{cat} and was calculated by Ergun (1952) relationship, which is expressed by Equation 17 as structured by Fogler (1999).

$$\frac{dP}{dW} = -10^{-5} \frac{1}{A_c \rho_b} \frac{G}{\rho_{gas} dp} \frac{(1-\varepsilon_b)}{{\varepsilon_b}^3} \left(\frac{b(1-\varepsilon_b)\mu}{dp} + aG\right) \quad (17)$$

In which A_c is the cross-sectional area of the bed in m², ρ_{gas} is the gas density in kg/m³, dp is the equivalent pellet diameter in m, G is the superficial mass flow in kg/(m²·s), and μ is the gas viscosity in kg/(m·s). The viscosity was calculated as described in Appendix A with values obtained from Reid et al. (1987).

The main difference between the axial-flow and radial-flow designs is expressed in Equation 17, as A_c is constant in the axial-flow design, while it is a function of W in the radial-flow design, as $A_c = 2\pi r$ and $W = \pi z \rho_b (r^2 - r_0^2)$, in which z represents the bed length, r represents the catalyst bed radial coordinate and r_0 the inner bed radius. The notation in which r is the catalyst bed radial coordinate is an exception throughout this paper, as it is used to denote different key variables in other occurrences. Hicks (1970) suggests using values of a and b as respectively 1.75 and 150 for $Re/(1-\varepsilon_b) < 500$, and 1.24 and 368 for $1000 < Re/(1-\varepsilon_b) < 5000$. As under the operational conditions presented in this study, $Re/(1-\varepsilon_b)$ was below 500 for the radial-flow reactor and slightly above 500 for the axial-flow, the values of a and b used were respectively 1.75 and 150 for both reactor models.

3.4. INTRAPARTICLE DIFFUSION

Models to describe heterogeneous kinetics considering intraparticle diffusion are extensively described in the literature (Elnashaie & Elshishini, 1993; Fogler, 1999; Froment & Bischoff, 1979). The generic model for the current study can be described by Equation 18.

$$\frac{1}{r^2}\frac{d}{dr}\left(r^2\frac{dP_{s,j}}{dr}\right) = -\frac{R_g T}{D_{e,j}} r_j \tag{18}$$

With boundary conditions given by Equations 19 and 20

$$P_{s,j} = P_j \quad \text{at } r = r_s \tag{19}$$

$$\frac{dP_{s,j}}{dr} \quad \text{at } r = 0 \tag{20}$$

In which, $P_{s,j}$ is the partial pressure of component *j* inside the catalyst, P_j is the partial pressure of component *j* in bulk condition, *r* is the pellet radial coordinate, r_s the value of the radius on the pellet surface in m, R_g is the ideal gases constant (8.314 x 10^2) in m^3·bar/(kmol·K), $D_{e,j}$ is the effective diffusion coefficient of the component *j* in m^2/h, and r_j is the rate of generation of the component *j* in kmol/(m^3·h). The effective diffusion coefficients were calculated using weighted binary molecular diffusivities and a tortuosity value of 3, as described in Appendix B.

This model is based on the following assumptions (Lee, 2005):

1. Interparticle diffusion resistance is negligible.
2. The catalyst pellet is isothermal.
3. Diffusion of a species in a pellet obeys Fick's first law and the effective diffusivities are invariant inside the particle.
4. The total pressure in the catalyst is uniform.
5. Steady-state condition holds.

The set of equations for each reacting component is presented by Equations 21-23.

$$\frac{1}{r^2}\frac{d}{dr}\left(r^2\frac{dP_{EB}}{dr}\right) = \frac{RT}{D_{e,EB}}[\varepsilon_s(r_{t1} + r_{t2} + r_{t3}) + \rho_s(r_{c1} + r_{c2} + r_{c3})] \tag{21}$$

$$\frac{1}{r^2}\frac{d}{dr}\left(r^2\frac{dP_{ST}}{dr}\right) = -\frac{RT}{D_{e,ST}}[\varepsilon_s r_{t1} + \rho_s(r_{c1} - r_{c4})] \tag{22}$$

$$\frac{1}{r^2}\frac{d}{dr}\left(r^2\frac{dP_{H_2}}{dr}\right) = -\frac{RT}{D_{e,H_2}}[\varepsilon_s(r_{t1} - r_{t3}) + \rho_s(r_{c1} - r_{c3} - 2r_{c4})] \tag{23}$$

In which, ε_s is the void fraction inside the catalyst, and ρ_s the catalyst density in kg/m^3.

The effectiveness factor of each reaction *i* is then calculated by Equation 24.

$$\eta_i = \frac{\int_0^V \left[\rho_s r_{ci}\left(P_{s,j}, T\right) + \varepsilon_s r_{ti}\left(P_{s,j}, T\right)\right] dV}{\left[\rho_s r_{ci}\left(P_{s,j}, T\right) + \varepsilon_s r_{ti}\left(P_{s,j}, T\right)\right] V} \tag{24}$$

In which, the thermal reactions r_{ti} as the catalytic reactions r_{ci} are a function of the partial pressures of the component inside the catalyst and temperature.

This set of intraparticle diffusion equations as well as the effectiveness factor were solved by orthogonal collocation. For the baseline problem, it was as performed by Lee & Froment (2008) with 6 internal collocation points, whereas in optimization routines, it was implemented with 3 internal collocation points.

3.5. ORTHOGONAL COLLOCATION

3.5.1. Theory

The methods for the solution of boundary value problems using orthogonal collocation were originally proposed by Villadsen & Stewart (1967) in which they distinguish three classes of methods: *Interior collocation*, *Boundary collocation*, and *Mixed*. The first method has been reported as more versatile as it can be used for non-linear differential equations and is the one applied in the current study for obtaining the effectiveness factors of heterogeneous reactions.

In problems such as diffusion or reaction in a cylindrical or spherical catalyst, or reaction in a packed bed reactor, the solution is symmetric about the center of the pellet or packed bed Finlayson (1973). For a symmetrical second-order boundary-value problem in one independent variable, *x*, in the region $x^2 < 1$, consider an unknown function y(x) which satisfies the linear or non-linear differential equation *L* over the volume *V* described by Equation 25 and boundary conditions by Equations 26 and 27.

$$L^{(V)}(y) = 0 \qquad \text{for } x^2 < 1 \tag{25}$$

$$y = y(1) \qquad \text{at } x = 1 \tag{26}$$

$$\frac{dy}{dx} = 0 \qquad \text{at } x = 0 \tag{27}$$

A suitable function that satisfies the boundary conditions is presented in equation 28.

$$y^{(n)} = y(1) + (1 - x^2)\sum_{i=0}^{n-1} a_i^{(n)} P_i(x^2) \tag{28}$$

In which, the $P_i(x^2)$ are polynomials of degree *i* in x^2, yet to be specified and $a_i^{(n)}$ are undetermined constants. Once $y^{(n)}$ has been adjusted to satisfy Equation 25 at *n* collocation points, the residual function $L^{(V)}(y)$ either vanishes everywhere or contains a polynomial factor of which zeros are in the collocation points.

These polynomials $P_i(x^2)$ are defined by the gaussian hypergeometric function in x^2, described by Equation 29, and the collocation points $x_1, \ldots, x_n$ are defined in the zeros of the polynomials $P_n(x^2)$, in which *n* corresponds to the number of collocation points. The parameter *a* is characteristic of the shape of the problem, being 1 for slabs, 2 for cylinders, and 3 for spheres.

$$P_i(x^2) = {}_2F_1(-i, i + {}^{a}/_{2} + 1, {}^{a}/_{2}) \tag{29}$$

Villadsen & Stewart (1967) present two alternatives to solving the problems. In the first approach, the polynomials are inserted into the set of differential equations and solved for the unknown coefficients $a_i^{(n)}$. In the second approach, an equivalent problem is formulated based on the unknown ordinates $y^{(n)}(x_i)$. The latter was adopted in the current study. These sets of equations are formulated using gradient and Laplacian operators for the function $y^{(n)}(x)$ described by Equations 30 and 31. Methods for obtaining matrices *A* and *B* are

described in detail in Villadsen & Stewart (1967) with examples for different geometries and numbers of collocation points.

$$\left.\frac{dy^{(n)}}{dx}\right|_{x=x_i} = \sum_{j=1}^{n+1} A_{i,j}\, y^{(n)}(x_j) \tag{30}$$

$$\left.x^{1-a}\frac{d}{dx}\left(x^{a-1}\frac{dy^{(n)}}{dx}\right)\right|_{x=x_i} = \sum_{j=1}^{n+1} B_{i,j}\, y^{(n)}(x_j) \tag{31}$$

The implementations of orthogonal collocation have been readily available to researchers and practitioners in a Python module (Leite, 2022b).

3.5.2. Application

Equations 18 were reformulated to dimensionless coordinates in the radial pellet dimensions, so that 0 < x < 1. Using the same notation as (Lee, 2005) this can be formulated as $\xi = r/r_s$ leading to Equation 32.

$$\frac{1}{\xi^2}\frac{d}{d\xi}\left(\xi^2\frac{dP_{s,j}}{d\xi}\right) = -\frac{{r_s}^2 R_g T}{D_{e,j}} r_j \tag{32}$$

And, combining to Equation 31, it is formulated a set of *n* nonlinear equations for each component. Considering three *k* reactant species, 3*n* equations. Notice that r_s is being used to denote the pellet radius while r_k to denote the rate of generation of component *k* in dimensionless coordinate ξ.

$$\sum_{j=1}^{n+1} B_{i,j}\, {P_{s,k}}^{(n)}(\xi_j) = \left.-\frac{{r_s}^2 R_g T}{D_{e,k}} r_k\right|_{\xi=\xi_j} \qquad \forall\, k \in EB, ST, H_2 \tag{33}$$

3.6. OPTIMIZATION

3.6.1. General problem formulation

Mathematically speaking, optimization is the minimization or maximization of a function subject to constraints on its variables (Nocedal & Wright, 2006). Luenberger & Ye (2008) divide optimization problems into two major categories: *linear programming*, and *nonlinear programming*. These categories are distinguished by the presence or not of nonlinear functions in either the objective function or constraints and lead to very distinct solution methods. A general constrained problem formulation can be stated as in Equation 34.

$$\begin{aligned} &\text{minimize} && f(\boldsymbol{x}) \\ &\text{subject to} && h_i(\boldsymbol{x}) = 0, \quad i \in \{1, 2, \dots, M\} \\ & && g_j(\boldsymbol{x}) \leq 0, \quad j \in \{1, 2, \dots, R\} \\ & && \boldsymbol{x} \in \Omega \end{aligned} \tag{34}$$

In which, $\boldsymbol{x}$ is a vector of decision variables of size *N* (also denoted optimization variables), *f* is the objective function, *h* and *g* are functional equality and inequality constraints respectively. Boundaries for each component of $\boldsymbol{x}$ might be explicit in the formulation when stating that $\boldsymbol{x} \in \Omega$, in which Ω is a set that defines limits for decision variables.

Throughout this work, due to the nature of the chemical engineering reaction design of the styrene reactor problem, *nonlinear programming* will be focused on. Two general paradigms of solutions will be discussed to such problems: Gradient-based algorithms, and Evolutionary algorithms. The first will be presented from a perspective of convex single-objective optimization with corresponding mechanisms for extending them to multi-objective problems. The second will be presented for general real-valued optimization problems.

3.6.2. Gradient-based algorithms

Gradient-based (or descent) algorithms are characterized by an iterative process in which one starts at an initial point; determines, according to a fixed rule, a direction of movement; and then moves in that direction to a (relative) minimum of the objective function on that line. At the new point, a new direction is determined, and the process is repeated (Luenberger & Ye, 2008).

There are two fundamental strategies for performing these iterations: *line search*, and *trust region*. In a sense, the line search and trust-region approaches differ in the order in which they choose the direction and distance of the move to the next iterate. Line search starts by fixing the direction and then identifying an appropriate distance. In trust region, we first choose a maximum distance, the trust-region radius, and then seek a direction and step that attain the best improvement possible subject to this distance constraint. If this step proves to be unsatisfactory, we reduce the distance measure and try again (Nocedal & Wright, 2006). In this study, line search methods will be addressed, of which several aspects and strategies will be described throughout this chapter.

In the line search strategy, the algorithm chooses a direction $\boldsymbol{p}_k$ and searches along this direction from the current iterate $\boldsymbol{x}_k$ for a new iterate with a lower function value.

$$\boldsymbol{x}_{k+1} = \boldsymbol{x}_k + \alpha_k \boldsymbol{p}_k \tag{35}$$

The distance to move along $\boldsymbol{p}_k$ can be found by approximately solving the following one-dimensional minimization problem to find a step length α.

$$\phi(\alpha) = f(\boldsymbol{x}_k + \alpha \boldsymbol{p}_k) \tag{36}$$

The methods for defining the step length α differ from unconstrained to constrained problems, therefore those will be addressed in the corresponding sub-sections.

3.6.2.1. Unconstrained Problems

Luenberger & Ye (2008) suggest that the first question that arises in the study of the minimization problem is whether a solution exists. The main result that can be used to address this issue is the theorem of Weierstras, which states that if the objective function is continuous and compact, a solution exists. Although recognizing this as a valuable result throughout the reasoning of *nonlinear programming* they present a primary concern with characterizing solution points and devising effective methods for finding them. And this is performed by defining optimality conditions.

The first and second-order *necessary conditions* for optimality are summarized as the following (Nocedal & Wright, 2006):

1) If $\boldsymbol{x}^*$ is a local minimizer and *f* is continuously differentiable in an open neighborhood of $\boldsymbol{x}^*$, then $\nabla f(\boldsymbol{x}) = 0$.
2) If the Hessian matrix of the objective *f* with respect to $\boldsymbol{x}$, $\nabla^2 f(\boldsymbol{x})$, exists and is continuous in an open neighborhood of $\boldsymbol{x}^*$, then $\nabla^2 f(\boldsymbol{x})$ is positive semidefinite.

The so-called *sufficient conditions* for optimality are analogous, however stating that $\nabla^2 f(\boldsymbol{x})$ is positive definite rather than positive semidefinite. A representation of a convex unconstrained problem and its respective true optimum is presented in Figure 3.

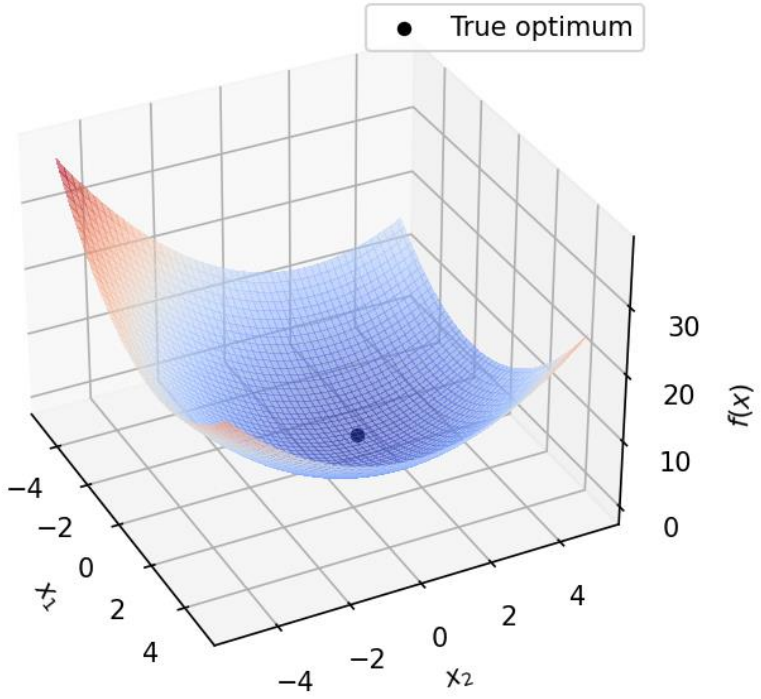

Figure 3 – Graphical representation of a quadratic function and its respective known true optimum.

With these definitions in mind, considering the iterative process of descent algorithms, two questions arise:

1) How to define the search directions.
2) How the define the step length in the best search direction.

Although *line search* methods first define the search direction and then define the step length, presenting these strategies in reverse order can be useful. Therefore, suppose there is a known best search direction at the current iteration $\boldsymbol{p}_k$.

In computing the step length α from equation 36, there is a tradeoff between precision and computational cost. Although it is desirable to obtain the best solution in the search direction, it can lead to a large number of function evaluations, which is usually undesirable, as these functions might be complex and computationally expensive. Therefore the most common strategy to define α is iteratively, by bracketing and interpolating, until some convergence conditions are satisfied.

The Wolfe conditions are probably the most common in unconstrained problems line search. They state that the value of the objective function must be smaller than a function of the original point (controlled by the parameter c_1) and so must be the curvature of the objective function (controlled by the parameter c_2). The suggestion of Nocedal & Wright (2006) is to use 1e-4 for c_1, and define c_2 as equal to 0.9 for Newton and Quasi-Newton methods, while 0.1 for Conjugate Directions and Steepest Descent. They are summarized by Equations 37 and 38, and visually represented by Figure 4, in which red points represent rejected step sizes and the green point an adequate step size.

$$\phi(\alpha) \leq \phi(0) + c_1 \alpha \phi'(0) \tag{37}$$

$$|\phi'(\alpha)| \leq -c_2 \phi'(0) \tag{38}$$

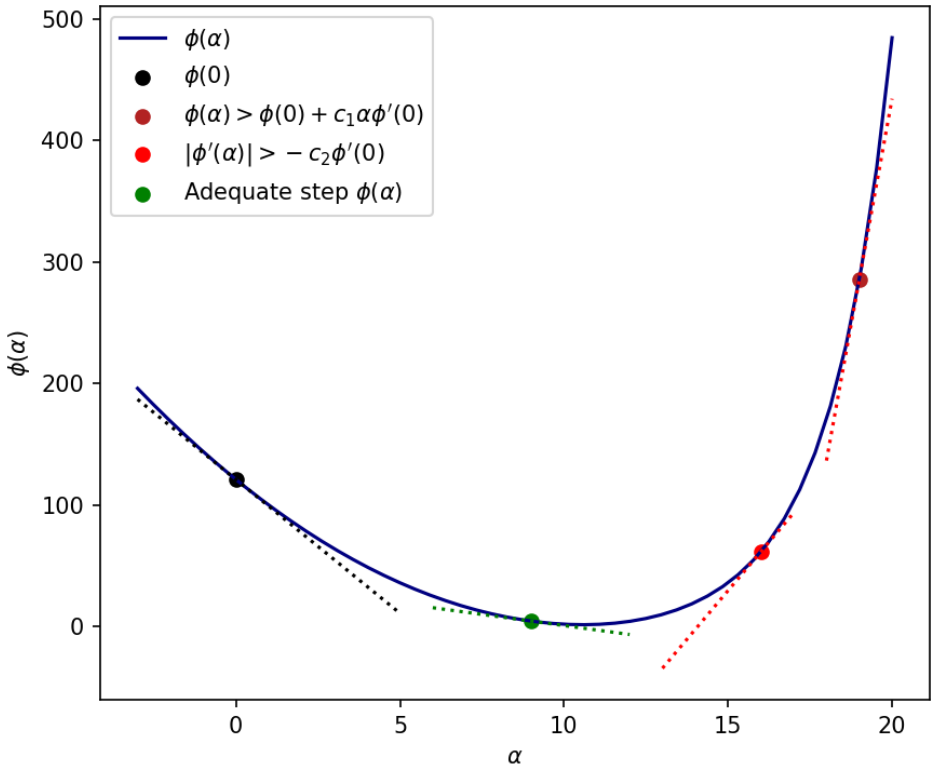

Figure 4 – Graphical representation of step size definition based on the Wolfe conditions.

Regarding the definition of the search direction, the steepest descent direction $-\nabla f(\boldsymbol{x}_k)$ is the most obvious choice for search direction for a line search

method. It is intuitive; among all the directions we could move from x_k it is the one along which *f* decreases most rapidly. However, it can be excruciatingly slow on difficult problems. (Nocedal & Wright, 2006).

Two broad categories of more efficient strategies to define the search directions compared to simply using the *steepest descent* are *conjugate directions* and *quasi-newton* methods (Nocedal & Wright, 2006). Throughout this work, only the latter will be discussed, as it is closely related to the constrained optimization algorithm applied to the styrene reactor problem.

The idea behind Newton's method is that the function *f* being minimized is approximated locally by a quadratic function, and this approximate function is minimized exactly. Thus, near $\boldsymbol{x}_k$ we can approximate f by the truncated Taylor series (Luenberger & Ye, 2008), leading to Equation 39.

$$f(\boldsymbol{x}) \simeq f(\boldsymbol{x}_k) + \nabla f(\boldsymbol{x}_k)(\boldsymbol{x} - \boldsymbol{x}_k) + \frac{1}{2}(\boldsymbol{x} - \boldsymbol{x}_k)^{\boldsymbol{T}}\nabla^{\boldsymbol{2}} f(\boldsymbol{x}_k)(\boldsymbol{x} - \boldsymbol{x}_k) \tag{39}$$

Therefore, the search direction $\boldsymbol{p}$, in the iteration of index *k*, is defined by Equation 40.

$$\boldsymbol{p}_k = -\nabla^2 f(\boldsymbol{x})^{-1}\nabla f(\boldsymbol{x}_k) \tag{40}$$

Which, in the case of quadratic functions, leads to the exact optimizer of the objective function *f*.

Quasi-Newton methods provide an attractive alternative to Newton's method in that they do not require computation of the Hessian and yet still attain a superlinear rate of convergence. In place of the true Hessian, they use an approximation B_k, which is updated after each step to take account of the additional knowledge gained during the step. The updates make use of the fact that changes in the gradient provide information about the second derivative of the objective along the search direction (Nocedal & Wright, 2006).

The most common strategies for Hessian updates are BFGS and SR1, summarized by Equations 42 and 43, in which $\boldsymbol{y}_k = \nabla f(\boldsymbol{x}_{k+1}) - \nabla f(\boldsymbol{x}_k)$ and $\boldsymbol{s}_k = \boldsymbol{x}_{k+1} - \boldsymbol{x}_k$.

$$\boldsymbol{p}_k = -{B_k}^{-1}\nabla f(\boldsymbol{x}_k) \tag{41}$$

$$B_{k+1} = B_k - \frac{B_k \boldsymbol{s}_k \boldsymbol{s}_k^T B_k}{\boldsymbol{s}_k^T B_k \boldsymbol{s}_k} + \frac{\boldsymbol{y}_k \boldsymbol{y}_k^T}{\boldsymbol{y}_k^T \boldsymbol{s}_k} \tag{42}$$

$$B_{k+1} = B_k + \frac{(\boldsymbol{y}_k - B_k \boldsymbol{s}_k)(\boldsymbol{y}_k - B_k \boldsymbol{s}_k)^T}{(\boldsymbol{y}_k - B_k \boldsymbol{s}_k)^T \boldsymbol{s}_k} \tag{43}$$

3.6.2.2. Constrained Problems

When dealing with constrained problems, a fundamental concept is the definition of an active constraint. An inequality constraint is said to be active at a feasible point $\boldsymbol{x}$ if it is equal to zero and inactive if greater than zero. By convention, we refer to any equality constraint as active at any feasible point (Luenberger & Ye, 2008).

Once defined what is an active constraint, one must notice that, considering an original search space $E^{(n)}$, the feasible search space is defined by a hypersurface of dimension *n-m*, in which *m* corresponds to the number of active constraints. This leads to a first-order condition analogous to the unconstrained equivalent. The gradient of the objective function projected in the tangent hyperplane of the feasible search space must be equal to zero in a local optimum.

Therefore, in the local minimum, $f(\boldsymbol{x}^*)$ is a linear combination of the gradients of active constraints, which leads to the introduction of Lagrange multipliers, and so, the *Lagrangian function*.

$$\mathcal{L}(\boldsymbol{x}, \boldsymbol{\lambda}, \boldsymbol{\mu}) = f(\boldsymbol{x}) + \boldsymbol{\lambda}^T \boldsymbol{h}(\boldsymbol{x}) + \boldsymbol{\mu}^T \boldsymbol{g}(\boldsymbol{x}) \tag{44}$$

In which, $\boldsymbol{\lambda}$ and $\boldsymbol{\mu}$ are vectors of the corresponding *Lagrange multipliers* of equality and inequality constraints. In this formulation, inequalities are stated as $\boldsymbol{g}(\boldsymbol{x}) \leq 0$, which leads to the condition of their corresponding *Lagrange multipliers* $\boldsymbol{\mu} \leq 0$. Therefore, the condition of *complementary slackness* is achieved for inactive inequality constraints by setting $\boldsymbol{\mu} = 0$, whereas for active constraints $\boldsymbol{g}(\boldsymbol{x}) = 0$.

And the analogous First-order and Second-order optimality necessary conditions for convex constrained optimization are:

1) $\nabla \boldsymbol{\mathcal{L}}(\boldsymbol{x}^*, \boldsymbol{\lambda}, \boldsymbol{\mu})$ with respect to $\boldsymbol{x}$ must be equal to zero with the *complementary slackness* condition respected.
2) $\nabla^2 \boldsymbol{\mathcal{L}}(\boldsymbol{x}^*, \boldsymbol{\lambda}, \boldsymbol{\mu})$ with respect to $\boldsymbol{x}$ must be positive semidefinite.

Nocedal & Wright (2006) classify algorithms for convex constrained optimization into *penalty functions* and *augmented Lagrangian*, *sequential quadratic programming*, and *interior-point methods*. Throughout this study, the algorithms of the second category were applied.

Sequential quadratic programming (SQP) is a collection of efficient constrained optimization algorithms with many similarities to the unconstrained *Newton* and *Quasi-newton method*s. These algorithms can be classified as *primal-dual* methods (Luenberger & Ye, 2008) as the search is performed in both *primal space* (decision variables) and *dual space* (Lagrange multipliers) simultaneously. A detailed review of SQP can be found at Boggs & Tolle (1996), in which, besides the line search approach, interior point methods are described.

In SQP algorithms, the main problem is approximated by a quadratic problem subproblem at each iteration, and the search direction is defined to be the solution to the subproblem defined by Equation 45 with minimization defined in terms of the search direction $\boldsymbol{p}_k$.

$$\begin{aligned} &\textit{minimize} && \frac{1}{2}\nabla_{xx}{}^2 \mathcal{L}(\boldsymbol{x}_k, \boldsymbol{\lambda}_k, \boldsymbol{\mu}_k)\boldsymbol{p}_k + \nabla f(\boldsymbol{x}_k)^T \boldsymbol{p}_k \\ &\textit{subject to} && \nabla \boldsymbol{h}(\boldsymbol{x}_k)^T \boldsymbol{p}_k + \boldsymbol{h}(\boldsymbol{x}_k) = 0 \\ & && \nabla \boldsymbol{g}(\boldsymbol{x}_k)^T \boldsymbol{p}_k + \boldsymbol{g}(\boldsymbol{x}_k) \leq 0 \end{aligned} \tag{45}$$

With these definitions stated, the search directions at each iteration can be represented by Equation 46, in which besides equality constraints, we have included active inequality constraints at an iteration *k*. Notice Luenberger & Ye (2008) when defining this equation do not distinguish equality from active inequality constraints, which, considering the definitions aforementioned of an active constraint, leads to the same formulation.

$$\begin{bmatrix} \boldsymbol{p}_{x,k} \\ \boldsymbol{p}_{\lambda,k} \\ \boldsymbol{p}_{\mu,k} \end{bmatrix} = \begin{bmatrix} \nabla_{\boldsymbol{xx}}{}^2\mathcal{L}(\boldsymbol{x}_k, \boldsymbol{\lambda}_k, \boldsymbol{\mu}_k) & \nabla \boldsymbol{h}(\boldsymbol{x}_k)^T & \nabla \boldsymbol{g}(\boldsymbol{x}_k)^T \\ \nabla \boldsymbol{h}(\boldsymbol{x}_k) & 0 & 0 \\ \nabla \boldsymbol{g}(\boldsymbol{x}_k) & 0 & 0 \end{bmatrix}^{-1} \begin{bmatrix} \nabla_{\boldsymbol{x}}\mathcal{L}(\boldsymbol{x}_k, \boldsymbol{\lambda}_k, \boldsymbol{\mu}_k) \\ \boldsymbol{h}(\boldsymbol{x}_k) \\ \boldsymbol{g}(\boldsymbol{x}_k) \end{bmatrix} \quad (46)$$

As in unconstrained problems, a line search strategy can be used, in which the values of both the primal and dual variables at the next iteration are defined by multiplying the search directions by a constant α, that satisfies some line search conditions. These can be stated as $\boldsymbol{x}_{k+1} = \boldsymbol{x}_k + \alpha_k \boldsymbol{p}_{x,k}$; $\boldsymbol{\lambda}_{k+1} = \boldsymbol{\lambda}_k + \alpha_k \boldsymbol{p}_{\lambda,k}$; and $\boldsymbol{\mu}_{k+1} = \boldsymbol{\mu}_k + \alpha_k \boldsymbol{p}_{\mu,k}$.

Rather than using Wolfe conditions in the line search, SQP algorithms use merit functions, in which only some degree of descent in the merit function value is necessary. Some examples of merit functions are presented by Nocedal & Wright (2006).

Notice the *Hessian* of the *Lagrangian function* with respect to $\boldsymbol{x}$, as in unconstrained problems, might be approximated by B_k, which is updated after each step. In the updates, rather than using the difference between gradients of the objective function, the differences between the gradients of the *Lagrangian function* with respect to $\boldsymbol{x}$ are used, such that $\boldsymbol{y}_k = \nabla_{\boldsymbol{x}}\mathcal{L}(\boldsymbol{x}_{k+1}, \boldsymbol{\lambda}_{k+1}, \boldsymbol{\mu}_{k+1}) - \nabla_{\boldsymbol{x}}\mathcal{L}(\boldsymbol{x}_k, \boldsymbol{\lambda}_k, \boldsymbol{\mu}_k)$.

SQP algorithms are based on active set strategies, therefore, general concepts of these strategies will be presented. The idea underlying active set methods is to partition inequality constraints into two groups: those that are to be treated as active and those that are to be treated as inactive. The constraints treated as inactive are essentially ignored.

At each step of the algorithm, a set of constraints termed the *working set* is to be treated as the active set. The working set is chosen to be a subset of the constraints that are actually active at the current point, and hence the current point is feasible for the working set. The algorithm then proceeds to move on the surface defined by the working set of constraints to an improved point. At this new point, the working set may be changed. Overall, then, an active set method consists of the following components: (1) determination of a current working set

that is a subset of the current active constraints, and (2) movement on the surface defined by the working set to an improved point (Luenberger & Ye, 2008).

Strategies for updating the working sets for SQP algorithms are presented in detail by Nocedal & Wright (2006). The expression *blocking constraints* is used by the authors to define constraints that potentially would be violated if a step $\mathbf{s}_k$ was taken in the primal space. This is performed by linear approximations of the currently *inactive* constraints in a given iteration. Blocking constraints are then recursively included in the active set if identified by the linear approximations. Conversely, based on the updates on the values of the *Lagrange multipliers*, some constraints should be removed from the active set to preserve the *complementary slackness*.

In the optimization of the styrene reactor, an SQP algorithm denoted *Sequential Least Squares Programming* (SLSQP) was applied. This algorithm was proposed by Kraft (1988) and follows the main ideas of SQP presented throughout this section with a primal-dual strategy, based on an active set, using merit functions in the line search, and damped BFGS *Hessian* approximations. When defining the search directions (equation 46) Kraft (1988) uses a *least-squares* method, the reason why the algorithm is denoted SLSQP rather than just SQP.

3.6.2.3. Applications to multi-objective problems

As described earlier, broadly speaking, there are two approaches to solving MOO problems. One approach is to transform the MOO problem into one or a series of single-objective problems (or sub-problems), and then solve the resulting problems by an established technique for single-objective. Two common techniques following this approach are weighted sum and ε-constraint. The second approach is the modification of single-objective techniques to solve problems with multiple objectives. It is referred to as the multi-objective approach. Techniques following this approach are metaheuristics (or stochastic algorithms) that are mostly population-based and include evolutionary algorithms (Rangaiah, et al., 2020).

The weighted-sum technique was applied to the styrene reactor problem in the current study when solving the optimization problem using convex methods due to comparable scales of the two objectives, conversion (yield) and selectivity. This strategy has been applied by other authors in chemical engineering problems such as Costa, et al. (2003) and Campos, et al (2018).

3.6.3. Evolutionary algorithms

3.6.3.1. Overview

Just as in nature, Evolutionary Operators operate on an evolutionary algorithm population attempting to generate solutions with higher and higher fitness. The three major operators associated with these algorithms are mutation, recombination (crossover), and selection (Coello, et al., 2007).

Throughout this study, variants of the algorithm GDE3 (Kukkonen & Lampinen, 2005) were used, therefore this literature review section will be focused on its operators. A comparison to the popular algorithm NSGA-II (Deb, et al., 2002) is presented in Appendix C. As previously mentioned, the variants of DE algorithms implemented are publicly available in a Python package (Leite, 2022a).

3.6.3.2. Initialization

The algorithms start initializing a population based on a user-specified number of individuals *N* and the boundaries of each decision variable. Each individual corresponds to a vector of optimization variables and several strategies can be adopted in this part. A usual strategy for this stage is to randomly sample points within the bounds of the problem. However, to improve the distribution of elements, Latin Hypercube Sampling was adopted as the initialization strategy, using *pymoo's* (Blank & Deb, 2020) implementation. To avoid initialization bias when comparing algorithms, the same predefined random generation seeds were used.

3.6.3.3. Differential Evolution

Differential Evolution was originally designed for single-objective optimization aiming to fulfill the following purposes (Storn & Price, 1997):

1. Ability to handle non-differentiable, nonlinear, and multimodal cost functions.
2. Parallelizability to cope with computationally intensive cost functions.
3. Ease of use: few control variables to steer the minimization. These variables should also be robust and easy to choose.
4. Good convergence properties: consistent convergence to the global minimum in consecutive independent trials.

In DE algorithms, at each generation, *N* new individuals – denoted *offspring* – are generated by performing parents' selection, mutation, and crossover. The general mechanism of DE is summarized in Figure 5.

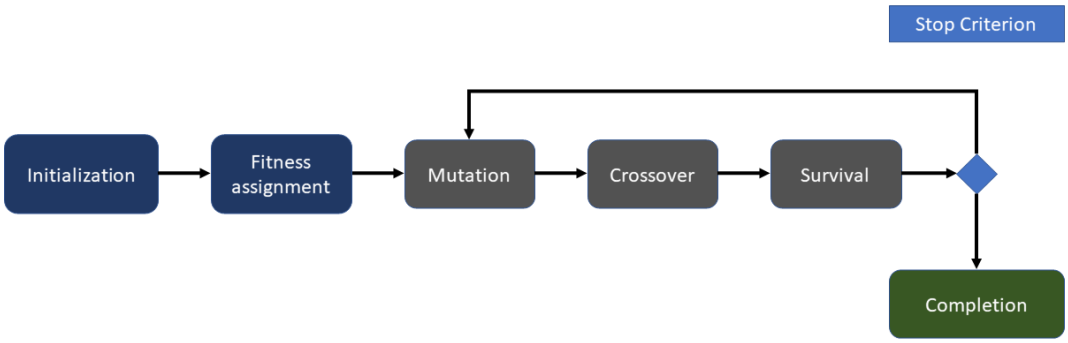

Figure 5 – General mechanism of Differential Evolution algorithm.

Different variants are proposed in the literature for DE operations, usually denoted DE/x/y/z, in which *x* corresponds to the mutation parent selection scheme, *y* to the number of difference vectors, and *z* to the crossover strategy. Using a MODE implementation inspired by NSGA-II, Babu & Anbarasu (2005) compared the performances of three usual variants: DE/rand/1/bin, DE/rand/1/exp, and DE/current-to-rand/1/bin in benchmark test problems. They observed that the first strategy performed better in both the Pareto set and diversity.

The creation of a new mutant vector $\boldsymbol{v}_i$ in the DE/rand/1 scheme is described by Equation 47 (Storn & Price, 1997), in which *F* is a scale parameter, usually denoted *mutation* parameter or *scale factor,* and $\boldsymbol{x}_{r1}$, $\boldsymbol{x}_{r2}$, and $\boldsymbol{x}_{r3}$ are vectors randomly selected from the current parent population mutually different and different from $\boldsymbol{x}_i$.

$$\boldsymbol{v}_i = \boldsymbol{x}_{r1} + F(\boldsymbol{x}_{r2} - \boldsymbol{x}_{r3}) \tag{47}$$

There are a few variants of equation 47. In our implementations, diversely from the original GDE3 (Kukkonen & Lampinen, 2005), *F* can be either a scalar or randomized within a range user-specified using uniform distribution dither. Jitter was additionally implemented with random uniform distribution, which adds rotation to difference vectors. In this study, it was used a deviation parameter $\gamma = 10^{-4}$ to add a small rotation, although still emphasizing preferred search directions. If a mutant vector is outside the problem boundaries, our algorithm

restores it using the bounce-back strategy. Setting parameter values equal to the bounds they violate should be avoided because it lowers the diversity of the difference vector population (Price, et al., 2005). If the component *j* of a mutant vector violates its boundaries $x_{j,l}$ or $x_{j,u}$, the bounce-back strategy replaces it with a value between the base vector $x_{j,r1}$ and the bound being violated, according to Equation 48.

$$v_{j,i} = \begin{cases} x_{j,r1} + rand(0,1)\left(x_{j,r1} - x_{j,l}\right), & \text{if} \quad v_{j,i} < x_{j,l} \\ x_{j,r1} + rand(0,1)\left(x_{j,u} - x_{j,r1}\right), & \text{if} \quad v_{j,i} > x_{j,u} \\ v_{j,i}, & \text{otherwise} \end{cases} \tag{48}$$

The mutation in single-objective DE is itself a self-adjusting phenomenon because the difference vectors are relatively large for the initial random population and, analogous to a noise term, progressively decay as the population gradually converges towards a single solution (Price, et al., 2005). Parameter *F* controls the speed and robustness of the search, i.e., a lower value for *F* increases the convergence rate but it also increases the risk of getting stuck into a local optimum (Kukkonen, 2007). In general, (survival) selection tends to reduce the diversity of a population, whereas mutation increases it. To avoid premature convergence, it is crucial that *F* be of sufficient magnitude to counteract this selection pressure (Price, et al., 2005). In the case of multi-objective optimization and conflicting objectives, lower control parameter values (e.g., 0.2) for *CR* and *F* can be used than in single-objective optimization because conflicting objectives already maintain diversity and restrain the search speed (Kukkonen, 2007). Uniform distribution dither in the range (0, 1] was successfully adopted by other authors in multi-objective variants of differential evolution (Babu, et al., 2005; Trivedi & Ramteke, 2021). For instance, when the emphasis on exploration is needed, such as in problems with discontinuous decision spaces, using higher limits can be useful. Conversely, to emphasize exploitation, using lower values for limits can improve results.

The amount of information inherited from either the corresponding parent $\boldsymbol{x}_i$ (target vector) or the mutant vector $\boldsymbol{v}_i$ is governed by a crossover parameter $CR \in [0, 1]$. In the classic binomial crossover scheme (Equation 49), random numbers in the range of [0, 1] are generated for each optimization variable of

index j for each trial vector $\boldsymbol{u}_i$. If the random number is smaller than CR, the optimization variable of index j of a new trial vector $\boldsymbol{u}_i$ is inherited from the mutant vector $\boldsymbol{v}_i$, else it is from the corresponding parent $\boldsymbol{x}_i$. An additional rule is used to ensure that each time at least one variable is inherited from the mutant vector, thus avoiding duplicates in the reproduction.

$$u_{j,i} = \begin{cases} v_{j,i}, & \text{if} \quad rand(0,1)_{j,i} < CR \quad \text{or} \quad j = j_{rand} \\ x_{j,i}, & \text{otherwise} \end{cases} \tag{49}$$

Price et al. (2005) analyzed several aspects of CR choice. Usually, objective functions that perform well with low values are decomposable - can be written as a sum of one-dimensional functions, while those that require values close to one are not. Choices of CR close to one are thus associated with the rotational invariance required for the algorithm and are dependent on the objective functions. Zaharie (2009) made a detailed study on the impact of crossover operators in DE. Her experiments illustrate the fact that the difference between binomial and exponential crossover variants is mainly due to different distributions of the number of mutated components. Furthermore, the behavior of exponential crossover variants was found to be more sensitive to the problem size than the behavior of variants based on the binomial crossover.

Some authors have adopted strategies that reinforce elitism when producing mutant vectors. Xue et al. (2003) proposed a DE selection and mutation variant that, in analogy to the single objective DE/best/1/bin, reinforces the selection characteristics of non-dominated individuals in the mutant vectors by a linear combination. In their implementation, if a target vector $\boldsymbol{x}_i$ is originally dominated, it is modified by linear combination with a randomly selected vector among non-dominated solutions. This strategy can be compared to the Following Heroes operation, incorporated in multi-objective DE by Trivedi & Ramteke (2021).

In contrast to selection schemes reinforcing elitism, Fan & Yan (2018) implemented an algorithm with an external archive population to reduce the loss of information. In their implementation, $\boldsymbol{x}_{r2}$ is selected from individuals of an external archive created from randomly selected individuals of the previous iteration. This allows $\boldsymbol{x}_{r2}$ to be chosen from dominated solutions, even though all

solutions of the main population in a generation might be non-dominated. Ensemble strategies have also been proposed in the literature and reported promising results in the context of single-objective DE in balancing exploration vs exploitation aspects of different selection strategies for mutation operators (Yi, et al., 2022).

In this study, besides the usual random parent selection (DE/rand), a strategy that reinforces elitism with simple operations and no additional control parameter proposed by Zhang et al. (2021) was evaluated on the reactor problem. Each solution in the current population has a rank assigned by non-dominated sorting (see section 3.6.3.5). Three parents of mutually exclusive indexes $\boldsymbol{x}_{r1}$, $\boldsymbol{x}_{r2}$, and $\boldsymbol{x}_{r3}$ are randomly selected for each mutation vector created. Then, positions are exchanged according to their ranks so that the best solution of the three (lowest rank) is assigned to $\boldsymbol{x}_{r1,}$ and the worst (highest rank) is assigned to $\boldsymbol{x}_{r3}$. This strategy was denoted as *ranked* in the current study and in *pymoode* (Leite, 2022a) to distinguish it from the usual random (*rand*) selection. When using high *CR* values there is a greater probability of trial vectors inheriting attributes from the corresponding mutant vectors. Therefore, in those situations, the *ranked* strategy can be especially useful. This advantage is considerably reduced when using low *CR* values, as most of the attributes of the trial vectors are inherited from the corresponding parents.

In single-objective DE, to decide if a trial vector $\boldsymbol{u}_i$ should become a member of the next generation, it is compared to the corresponding target vector $\boldsymbol{x}_i$ using a greedy criterion (Storn & Price, 1997). This one-to-one comparison might be inadequate in multi-objective problems and is usually replaced by other survival strategies.

Survival strategies in multi-objective differential evolution can be classified into three categories (Cheng, et al., 2016). The first type preserves the rigorous one-to-one (survival) selection scheme proposed by single-objective DE. In methods of the second type, the parent population is first combined with the offspring then the united population is truncated into the original size. It is sometimes denoted ($\mu + \lambda$), in which μ is the number of members in the parent population and λ, the number of members in the *offspring* (Deb, 2001). The third type is a mix of the above two schemes. The one-to-one selection is first performed if two competed solutions are comparable; otherwise, the two

solutions enter the population for later sorting at the end of the iteration using a united population selection procedure.

In GDE3, the hybrid type is used, which can be useful for avoiding premature convergence when associated with low *CR* values. According to Cheng et al. (2016), it performs better than the two other schemes. The ($\mu + \lambda$) is adopted in NSDE (Iorio & Li, 2004), whereas the one-to-one selection is preserved in PDE (Abbass, et al., 2001).

3.6.3.4. Constrained-Domination

The concepts of sorting and survival are based on the concept of domination, and, in the context of constrained problems, the concept of constrained domination.

According to Deb (2001), one solution x_1 dominates another x_2 if:

1. x_1 is no worse than x_2 in all objectives.
2. x_1 is strictly better than x_2 in at least one of the objectives.

And the constrained-domination rule for MOO problems proposed by Deb et al. (2002), when comparing two solutions, x_1 is said to constrained-dominate x_2 if any of the following conditions is true:

1. Solution x_1 is feasible and x_2 is not.
2. Solutions x_1 and x_2 are both infeasible, but solution x_1 has a smaller overall constraint violation.
3. Solutions are feasible and solution x_1 dominates solution x_2.

3.6.3.5. Sorting

Sorting concepts apply to the initial population in a fitness assignment stage and the combined *parent* and *offspring* population in the survival stage of each generation. The Rank and Crowding survival strategy of NSGA-II aims to assign fitness to population members based on non-dominance sorting and preserving diversity (Deb, et al., 2002). The same operator is originally adopted in GDE3 (Kukkonen & Lampinen, 2005) when truncating the population size.

Each solution is assigned a fitness (rank) according to non-domination criteria, considering objective functions and constraints. Ranks are sorted in ascending order from the best to the worst solutions. This occurs in a process denoted *Non-dominated sorting* (Deb, et al., 2002). Once the reproduction operators increase population size at each generation, algorithms that use a fixed number of individuals need some operation for truncating the population into its original size. In the *Rank and Crowding* survival of NSGA-II, ranks are the first criterion for selecting individuals that proceed into the next generation. When exceeding the population size, individuals with the same rank are sorted using a crowding distance metric based on their distance to their neighbors in the objective space. This process is precisely described by Deb et al. (2002).

Kukkonen & Deb (2006a) verified that the original truncating strategy of NSGA-II can reduce the diversity of solutions in some situations. To address this issue, they proposed an algorithm that first calculates crowding distances for the members of a non-dominated set. Then, instead of selecting n members having the largest values, members having the smallest values are removed one by one, updating the crowding distances for the remaining members of the set after each removal.

Other strategies for preserving diversity have proven more successful in guiding the survival stage for problems with more than two objectives. Kukkonen & Deb (2006b) proposed a version of GDE3 that uses a crowding metric based on the Euclidean distances to the M nearest neighbors (M-NN). Strategies based on rank and reference directions (Deb & Jain, 2014; Jain & Deb, 2014) have also been successful in three-objective optimization. Reddy & Dulikravich (2019) proposed an algorithm that combines differential evolution mating operations to reference direction-based survival, denoted NSDE-R. It was also implemented

and compared to GDE3 with the *M*-NN survival strategy. In NSDE-R, the Das Dennis reference directions were used with 18 partitions.

3.6.3.6. Implementation

In this study, GDE3 was implemented as an independent algorithm using *pymoo's* basic structure. During this study, the *pymoo* version was 0.5.0. Our implementations are publicly available in the Python package *pymoode* (Leite, 2022a).

The following steps can summarize GDE3:

1. Initialize a population of size *N*.
2. Apply non-dominated sorting to assign fitness to the population.
3. While the termination criteria are not met:
   - 3.1. Generate *offspring* individuals:
     - 3.1.1. Select vectors $\boldsymbol{x}_{r1}$, $\boldsymbol{x}_{r2}$, and $\boldsymbol{x}_{r3}$ from the parent population.
     - 3.1.2. Create mutation vectors $\boldsymbol{v}_i$ by DE operations.
     - 3.1.3. Generate offspring individuals $\boldsymbol{u}_i$ by performing binomial crossover between mutation and target vectors $\boldsymbol{v}_i$ and $\boldsymbol{x}_i$.
     - 3.1.4. Perform a one-to-one comparison before truncating.
   - 3.2. Truncate the population into the original size based on sorting criteria (dominance and crowding metric).

4. METHODS

4.1. REACTOR MODELING

In the reactor simulations, it was adopted the set of fundamental equations described in detail in sections 3.2 to 3.5. The four reactions from section 3.2 were used to formulate continuity equations of an ODE system. Additionally, as described in section 3.3, the fundamental equations present in the literature were used to describe energy balance, pressure drop, and intraparticle diffusion. The complete heterogeneous solution is computationally expensive, although more precise from a fundamental perspective compared to its corresponding pseudohomogeneous variant. Therefore, when comparing MOEAs in Appendix C it was adopted a pseudohomogeneous simplification (Dimian & Bildea, 2019; Lee, 2005), which in our current implementation takes about the one-sixteenth time of the complete model. A simplified representation of the modeling elements for a single catalyst bed is presented in Figure 6. All inlet values for the first catalyst bed in a reactor are user-specified. Whereas for the others in sequence, the inlet values of pressure and molar flow rates are defined using the outlet values from previous beds, except for the inlet temperature, which is user-specified. The complete simulation program is available in a public code repository (Leite, 2022c).

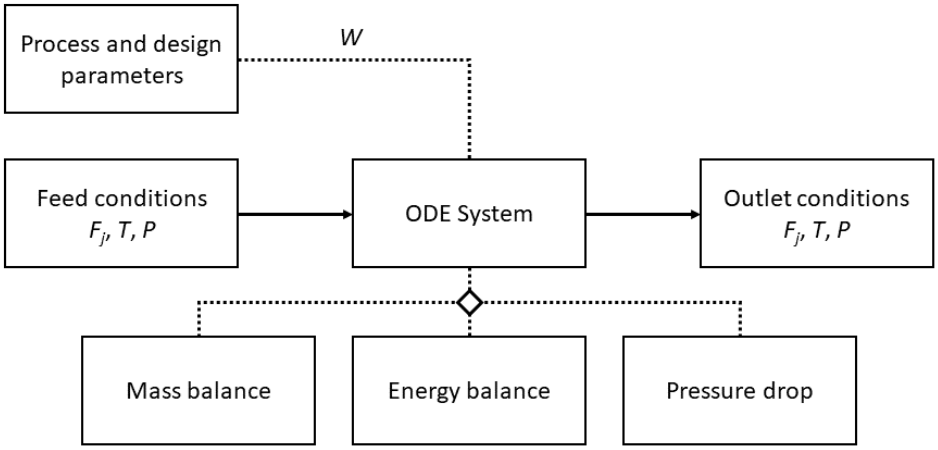

Figure 6 – Simplified representation of the modeling elements for a single catalyst bed.

4.2. BASELINE REACTOR DESIGN

The baseline reactors considered in this study were adiabatic reactors with three catalyst beds, and intermediate heating but no intermediate injection of steam or any other component. Dimensions and inlet operational conditions were defined using the same values as Lee & Froment (2008) for simulations at original conditions. They are presented in Table 2, Table 3, and Table 4. When performing optimization, possibilities of changing the number of catalyst beds, dimensions, and inlet operational conditions were explored. These changes are explained in detail in section 4.3.

Table 2 – Reactor dimensions and inlet operational conditions.

	Value					
	Axial-flow			Radial-flow		
Parameter	Bed 1	Bed 2	Bed 3	Bed 1	Bed 2	Bed 3
W [kg]	72950	82020	78330	72950	82020	78330
Inner radius [m]	3.5	3.5	3.5	1.5	1.5	1.5
Length [m]	1.33	1.50	1.43	7	7	7
Inlet *T* [K]	886	898.2	897.6	886	898.2	897.6
Inlet *P* [bar]	1.35*			1.25		
Inlet F_{H2O}/F_{EB}	11			11		
Inlet F_t [kmol/h]	8496.37			8496.37		

*The original pressure used by Lee & Froment (2008) was 1.25 bar, but it was redefined to 1.35 bar to result in outlet pressure of approximately 0.5 bar.

Table 3 – Individual components' inlet molar flow rates.

Component	Inlet molar flow rate [kmol/h]
EB	707.0
ST	7.104
BZ	0.293
TO	4.968
H_2O	7777

Table 4 – Properties of catalyst beds.

Property	Symbol	Unit	Value
Bed bulk density	ρ_b	kg/m³	1422
Catalyst solid density	ρ_s	kg/m³	2500
Bed bulk void fraction	ε_b		0.4312
Catalyst solid void fraction	ε_s		0.4
Equivalent pellet diameter	*dp*	m	0.055
Tortuosity factor	τ		3

Substantial differences occur when comparing the reactor specifications adopted in the current study and previous literature (Babu & Anbarasu, 2005; Yee, et al., 2003; Gujarathi & Babu, 2010; Tarafder, et al., 2005; Chaudhari, et al., 2022). Some of the most relevant points are listed below.

- Vacuum operation versus positive pressure (baseline absolute inlet pressure of 2.4 bar).
- Radial-flow versus axial-flow design.
- Intermediate heating versus intermediate steam injection.
- The number of catalyst beds.
- Total ethylbenzene molar feed rate.

Vacuum operation and radial-flow design are usual in industrial practice (Chen, 2006). Both are related to considerably superior performance due to the benefits of operating at lower pressures (Leite, et al., 2021). The decision-making processes related to steam-to-ethylbenzene feed ratios in reactors with intermediate heating or intermediate steam injection are considerably different. In the first situation, inlet temperatures of each stage are not direct consequences of steam injection, whereas this occurs in intermediate steam injected operation. Therefore, both reactor designs are considerably different from a modeling perspective. Both two and three individual catalyst beds are usual in industrial design (Li, 2007; ENI-Versalis, s.d.), although they also lead to distinct reactor models. As the reactor design previously adopted by previous studies focused on MOEAs was considerably different, limitations in ethylbenzene feed rates are evident, as previous studies considered a base total ethylbenzene feed rate of 36.87 kmol/h versus 707 kmol/h adopted.

4.3. OPTIMIZATION PROBLEM

In the dehydrogenation reactor, obtaining maximum ST conversion (yield) denoted X_{ST}, and selectivity denoted S_{ST} is desirable. These are conflicting objectives as increasing conversion increases the production of byproducts, lowering selectivity. Therefore, it can be structured as a multi-objective optimization problem with the objective functions described by Equations 50 and 51. In this study, both objectives were implemented as minimization problems of their negative values to follow a conventional optimization problem formulation.

$$X_{ST} = \frac{F_{out,ST} - F_{in,ST}}{F_{in,EB}} \tag{50}$$

$$S_{ST} = \frac{X_{ST}}{F_{in,EB} - F_{out,EB}} \quad (51)$$

In which, $F_{out,j}$ is the outlet molar flow rate of component *j* in kmol/h and $F_{in,j}$ is the inlet molar flow rate of component *j* in kmol/h.

In multiobjective optimization problems, the conflicting objective functions can be combined by a weighted sum technique, as described by Rangaiah, et al. (2020) and performed by Costa, et al. (2003) and by Campos, et al. (2018). When comparing axial to radial flow reactor design, this approach was adopted and the two objective functions were combined in single objective subproblems with the objective function f_{ws}, described by Equation 52, to either select relevant solutions by weighted sum criteria (for multi-objective algorithms), or to define SOO subproblems.

$$f_{ws} = -[w_1 S_{ST} + (1 - w_1) X_{ST}] \quad (52)$$

In which, w_1 assumes values from 0 to 1, producing an efficient frontier with different weights for the conflicting objective functions.

The best scenario for each industrial unit must consider its unique capability of performing other processes, the cost of raw materials, and utility consumption. However, these scenarios are somehow encompassed by the Pareto optimal solutions in terms of single-pass conversion and selectivity for reactor operation. Section 5 will present relevant qualitative aspects of the plantwide decision processes. Working at lower conversion and higher selectivity levels implies less fresh ethylbenzene consumption per unit of styrene produced, whereas higher separation and recycling costs. This strategy has been considered adequate in the economic analysis performed by Luyben (2011). In contrast, in a different context (Sundaram, et al., 1991), the optimized economic returns of an existing plant were obtained for higher single-pass conversion.

Catalyst deactivation is a complex phenomenon as it occurs by several mechanisms concurrently. In most cases, catalyst aging is caused by carbon deposition on the catalyst, chemical decomposition of the active ingredient in the catalyst, and mechanical disintegration of catalyst particles (Chen, 2006).

Temperature and partial pressure gradients have been reported to influence potassium migration leading to deactivation (Meima & Menon, 2001). These gradients are expected to be more pronounced when operating at high single-pass conversion as the reaction rates are necessarily increased, which influences transport phenomena inside the catalyst.

In future work, other objectives might be incorporated into the problem if plantwide operations are considered (furnaces, heat exchangers, decanter, and distillation columns). For instance, a multi-objective optimization problem could consider plantwide utility consumption, atmospheric emissions, capital costs, and other economic aspects. In the reactor, as an isolated unity, energy requirements are primarily due to process steam generation and recycling unreacted ethylbenzene. The author suggests referring to Dimian & Bildea (2019) and Luyben (2011) for examples of plantwide integrated studies.

The optimization variables considered were the inlet pressure on the first catalyst bed P_{in} [bar], inlet temperature T_i [K], and catalyst loading W_i [kg] of each bed of index i. It is important to remark that, in the optimization process, as the bed bulk density was set with a constant value, bed dimensions were changed as a consequence of changes in catalyst loading. In radial-flow beds, bed length and inner radius were preserved, while changes in catalyst loading had an impact on the outer radius. And in the axial-flow beds, the cross-sectional radius was preserved, while changes in catalyst loading led to changes in bed length.

From a modeling and optimization perspective, a greater cross-sectional area would result in a lower pressure drop. Considering our problem is limited by the outlet pressure, the best reactor performance would (mathematically) occur, for a given catalyst loading, with the maximum values for inner radius, when considering axial-flow design, and both inner radius and length, when considering radial-flow, as the reactor would operate with the lowest overall pressure. However, reactor design should consider other aspects to limit these values, such as the flow distribution. Li (2007) presents alternatives for scaling up and some associated issues. To adopt a conservative approach, it was decided to preserve the original values of the dimensions related to the cross-sectional area, whereas allowing the dimensions related to bed depth to change according to catalyst loading. This approach is similar to the one adopted in the simulations performed by Lee & Froment (2008).

Limits for pressure were defined to avoid infeasible solutions, in which starting from low initial pressures, the pressure drop leads to negative absolute pressures. As the pressure drop changes according to catalyst bed type, the lower bounds for inlet pressure able to prevent infeasible solutions were set with different values for either radial-flow or axial-flow reactors. In experiments varying inlet steam-to-ethylbenzene ratios, boundaries for inlet pressure were selected after numerical simulations using different ranges for each steam ratio. The selected values would produce feasible solutions but near the operational limit, considering the outlet pressure constraint (Equation 53) and the limits of other decision variables. The strategy was based on the minimum and maximum pressure drop occurring with the minimum and maximum catalyst loading and temperature for a given steam ratio. Therefore, the choice of inlet pressure boundaries would foster convergence when sampling the initial population but would not create active boundaries in the final solutions.

The boundaries for catalyst loading were defined to preserve dimensions in a range close to the original values reported by Lee & Froment (2008), thus avoiding inconsistent scaling up. The upper bounds for temperatures were defined based on process limitations and lower bounds to ensure algorithm convergence.

When using gradient-based algorithms, the choice of initial estimation for decision variables plays a major role. The convergence using different combinations of values was tested in pseudo-homogeneous reactors using effectiveness factors $\eta = 1$, and then a set of values that had converged properly was retained. The same initial guesses were used at all points of the Pareto fronts.

The boundaries and initial guesses for the optimization variables are presented in Table 5.

Table 5 – Boundaries and initial guesses for optimization variables.

Variable	Lower bound	Upper bound	Initial guess
W_1 [kg x 10^3](2)	72.5	85.0	73.0
W_2 [kg x 10^3]	72.5	85.0	73.0
W_3 [kg x 10^3]	72.5	85.0	73.0
T_1 [K](2)	800.00	913.15	900.00
T_2 [K]	820.00	913.15	910.00
T_3 [K]	840.00	913.15	913.15
P_{in} [bar] axial-flow	1.20	2.50	1.40
P_{in} [bar] radial-flow(3)	0.60	2.00(1)	1.10

(1) The upper boundary was readjusted to 0.8 when using evolutionary algorithms.
(2) Removed in the two-bed reactor configuration.
(3) Narrower ranges were adjusted when changing steam-to-ethylbenzene ratios or the number of catalyst beds.

As there is pressure drop along catalyst beds, and there is an industry limitation as to the lowest practicable pressure, constraints for outlet pressure must be considered. It was adopted 0.5 bar as the outlet pressure limit, following values reported by Rase (2000), although reactors operating at lower pressures (41 kPa) have been reported (Chen, 2006).

$$0.5 \leq P_{out} \tag{53}$$

In which P_{out} corresponds to pressure at the outlet of the reactor in bar.

When comparing axial to radial flow design, it was preserved the inlet steam-to-ethylbenzene ratio used by Lee & Froment (2008) once verified that, if included as an additional decision variable, it would necessarily converge to its upper boundaries for any different weights for conversion and selectivity. However, it is a significant heat consumer in the reactor, and its impact on conversion and selectivity must be considered in industrial decision-making. It was addressed in the experiments using evolutionary algorithms (which considered only radial-flow reactors) by two different approaches.

1. The steam-to-ethylbenzene molar feed ratio (S-EB) was set at distinct discrete levels: 7, 9, 11, 13, and 15. For each, the Pareto optimal solutions in terms of conversion and selectivity were found.

2. S-EB was included as both an additional decision variable and objective, which turns the problem into a three-objective problem. This approach has the advantage of lesser computational cost and continuous values for the steam ratio in the Pareto optimal solutions. In contrast, it reduces selective pressure for maximizing conversion and selectivity.

Furthermore, in experiments comparing reactor design, it was verified that the lower boundaries of this problem might produce solutions in a region of too low conversion (Leite, et al., 2021), therefore undesirable from an industrial perspective. To address this issue, in experiments with evolutionary algorithms, it was included an additional constraint to create a lower limit for single-pass conversion of 50%. By including this constraint, the feasible space was reduced removing a region undesirable from an industrial perspective due to the small single-pass conversion. Considering the constraint handling strategy adopted, this would reinforce exploiting the region of the most interest as the solutions with both the outlet pressure greater than 0.5 and conversion greater than 50% would be preferred over solutions with any of these conditions violated.

$$0.5 \leq X_{ST} \tag{54}$$

4.4. NUMERICAL ROUTINES

The system of differential equations of each bed instance was solved using an Explicit Runge-Kutta method of order 5 with errors based on order 4, from the *solve_ivp* function of *scipy.integrate* module. The system of nonlinear equations for the orthogonal collocation points was solved using both the Levenberg-Marquardt and Powell's hybrid algorithms from the *root* function of *scipy.optimize* module. The first was used at the entrance of the reactor where good initial estimations for solutions were not available and convergence was difficult. The latter was used for other points, in which the solutions from previous points were good initial estimations and convergence was adequate and fast. The optimization for the nonlinearly constrained single-objective subproblems was solved using the 'SLSQP' algorithm from the *minimize* function of *scipy.optimize* module. The *scipy* version used in this study was 1.7 (Jones, et al., 2001-).

Orthogonal collocation was implemented by the author throughout a published article (Leite, et al., 2021) using Python 3 basic language. The implementation was later made available to users in a public repository denoted *collocation* (Leite, 2022b).

As aforementioned, the evolutionary algorithms were implemented by combining basic structures from *pymoo* (Blank & Deb, 2020) with novel structures implemented by the author and made publicly available in the code repository and Python package *pymoode* (Leite, 2022a).

4.5. EVOLUTIONARY ALGORITHM EXPERIMENTS

The experiments presented in this dissertation's main body focus on applying GDE3 to the styrene reactor problem and the fundamental analysis of the results. Additional experiments to define control parameters and a comparison to the peer algorithm NSGA-II (Deb, et al., 2002) are provided in Appendix C.

In short, GDE3 had its best performance using a high crossover parameter of 0.9 (for binomial crossover), which increases the rotational invariance of the algorithm. This attribute is beneficial in this problem due to the interdependence

of decision variables in the objective functions. The same characteristic of the problem is probably associated with the superior performance of the DE reproduction operators compared to NSGA-II. Moreover, a simple method for exploiting Pareto dominance in GDE3 parent selection improved its convergence speed without reducing population diversity.

Considering these results, the choices for hyperparameters in the main experiments were the following:

- F: [0.0, 1.0]
- CR: 0.9
- DE/rand/1/bin
- Jitter deviation parameter γ: 10^{-4}

For all two-objective problems, the modified pruning removal strategy in survival by Kukkonen & Deb (2006a) was adopted, whereas, for the three-objective problem, GDE3 was modified by the M-NN survival strategy (Kukkonen & Deb, 2006b).

Single-run experiments were performed, considering the computational costs of the complete heterogeneous model adopted. A population size of 100 was used in individual two-objective experiments with different steam-to-ethylbenzene molar feed ratios, and optimization was terminated within 100 generations. The number of generations was selected after numerical experiments using the pseudohomogeneous model. It is possible to verify in Appendix C that it provides adequate convergence. It was chosen a population of 200 and 150 generations for the three-objective problem.

Future work might incorporate surrogate models to reduce the computational cost associated with objective function evaluations. This strategy has been applied to chemical processes by other authors who verified a reduction from 2 to 5 in the number of simulations (Beck, et al., 2015). Performance metrics to define search termination and taboo list to avoid re-visits have been successful in chemical engineering problems (Sharma & Rangaiah, 2013) and can reduce the number of function evaluations.

5. RESULTS AND DISCUSSION

5.1. BASELINE SIMULATION PROBLEM

5.1.1. Energy balance validation

To verify the numerical solution consistency, the outlet values obtained using the same dimensions and operating conditions as Lee & Froment (2008) were compared to those reported in their study. However, the values obtained were significantly different in terms of outlet temperature and ST selectivity. Then, to verify the consistency of the results obtained in this study and of those obtained by Lee & Froment (2008), the energy balance was checked at the inlet and outlet of the first catalyst bed using each of the results. The energy balance for adiabatic operation at steady-state can be expressed by Equation 55.

$$\dot{E}_{gen} = \sum_{j} F_{out,j} \Delta H_{out,fj} - \sum_{j} F_{in,j} \Delta H_{in,fj} = 0 \tag{55}$$

In which, $\dot{E}_{gen}$ is the energy generation rate in kJ/h, $\Delta H_{out,fj}$ is the heat of formation of component *j* in the outlet in kJ/kmol, and $\Delta H_{in,fj}$ is the heat of formation of component *j* in the inlet in kJ/kmol. The values of heat of formation ΔH_{fj} of component *j* at temperature *T* were calculated based on Reid, et al. (1987). The term $\dot{E}_{gen}$ conceptually is equal to zero, as the system operates at steady-state, and any differences are a consequence of mathematical and/or numerical errors.

Lee & Froment (2008) simulated axial-flow and radial flow reactors using a feed pressure of 1.25 bar, dimensions, and other inlet values presented in Table 2. The same was performed in the current to verify numerical solutions' consistency. Results for the first bed of each reactor are presented in Table 6.

Table 6 – Comparative results to verify the consistency of the energy balance.

Lee & Froment (2008)						
	X_{EB} %	S_{ST} %	S_{BZ} %	S_{TO} %	T_{out}	$\dot{E}_{gen}$ [kJ/h]
Axial-flow	36.89	98.49	1.00	0.51	811.36	-6.91 x 10^6
Radial-flow	36.59	98.43	1.01	0.56	812.04	-6.85 x 10^6
Current study						
	X_{EB} %	S_{ST} %	S_{BZ} %	S_{TO} %	T_{out}	$\dot{E}_{gen}$ [kJ/h]
Axial-flow	35.84	95.93	1.12	2.95	827.65	-2.62 x 10^3
Radial-flow	35.85	95.97	1.11	2.92	827.60	-2.59 x 10^3

The values of $\dot{E}_{gen}$ were compared to the heat of reaction of the main reaction to verify their magnitude. The heat of reaction of the main reaction corresponds to 1.2486 x 10^5 kJ/kmol of EB consumed at 900K and to 1.2464 at x 10^5 kJ/kmol of EB consumed at 850K. Using conversion, selectivity, and outlet temperature reported by Lee & Froment (2008), the values of $\dot{E}_{gen}$ correspond to the enthalpy change of more than 50 kmol/h of EB converted into ST, which is more than 19% of the total amount converted in the first bed, respectively 257 kmol/h and 255 kmol/h in the axial-flow and radial-flow reactors. In contrast, the values of $\dot{E}_{gen}$ obtained in this study correspond to approximately 0.01% of the total amount of EB converted into ST in the first bed of each reactor. Thus, in terms of energy balance consistency, the solutions presented in the current study can be considered reliable, while perhaps those obtained by Lee & Froment (2008) converged to imprecise results.

Although the reactor simulations presented by Lee & Froment (2008) show inconsistency concerning the energy balance, the parameter estimation performed in their study proved to be consistent once the plots of components' profiles under experimental conditions match reproductions performed during the current study using the estimated parameters.

5.1.2. Simulation results

The reactors at sub-optimal operating conditions were simulated with dimensions, and inlet values presented in Table 2. The inlet pressure of the axial-flow reactor was defined as 1.35 bar instead of 1.25 bar, to result in an outlet pressure close to 0.5 bar. Reactors were evaluated in terms of cumulative conversion of EB, ST, BZ, and TO; outlet temperature T_{out}; and outlet pressure P_{out}. The cumulative conversion of each component j is noted as X_j. The results obtained are presented in Table 7 and Figure 7.

Table 7 – Results obtained for different reactor configurations at sub-optimal conditions.

	Reactor					
	Axial-flow			Radial-flow		
	Bed 1	Bed 2	Bed 3	Bed 1	Bed 2	Bed 3
X_{EB} %	35.8	66.6	84.9	35.8	65.6	83.2
X_{ST} %	34.4	59.8	71.4	34.4	58.4	66.4
X_{BZ} %	0.40	1.02	1.61	0.40	1.03	1.75
X_{TO} %	1.06	5.76	11.9	1.05	6.18	15.0
S_{ST} %	95.9	89.8	84.1	96.0	89.0	79.8
P_{out} [bar]	1.162	0.887	0.481	1.225	1.196	1.166
T_{out} [K]	827.6	858.5	858.5	827.6	861.3	861.3

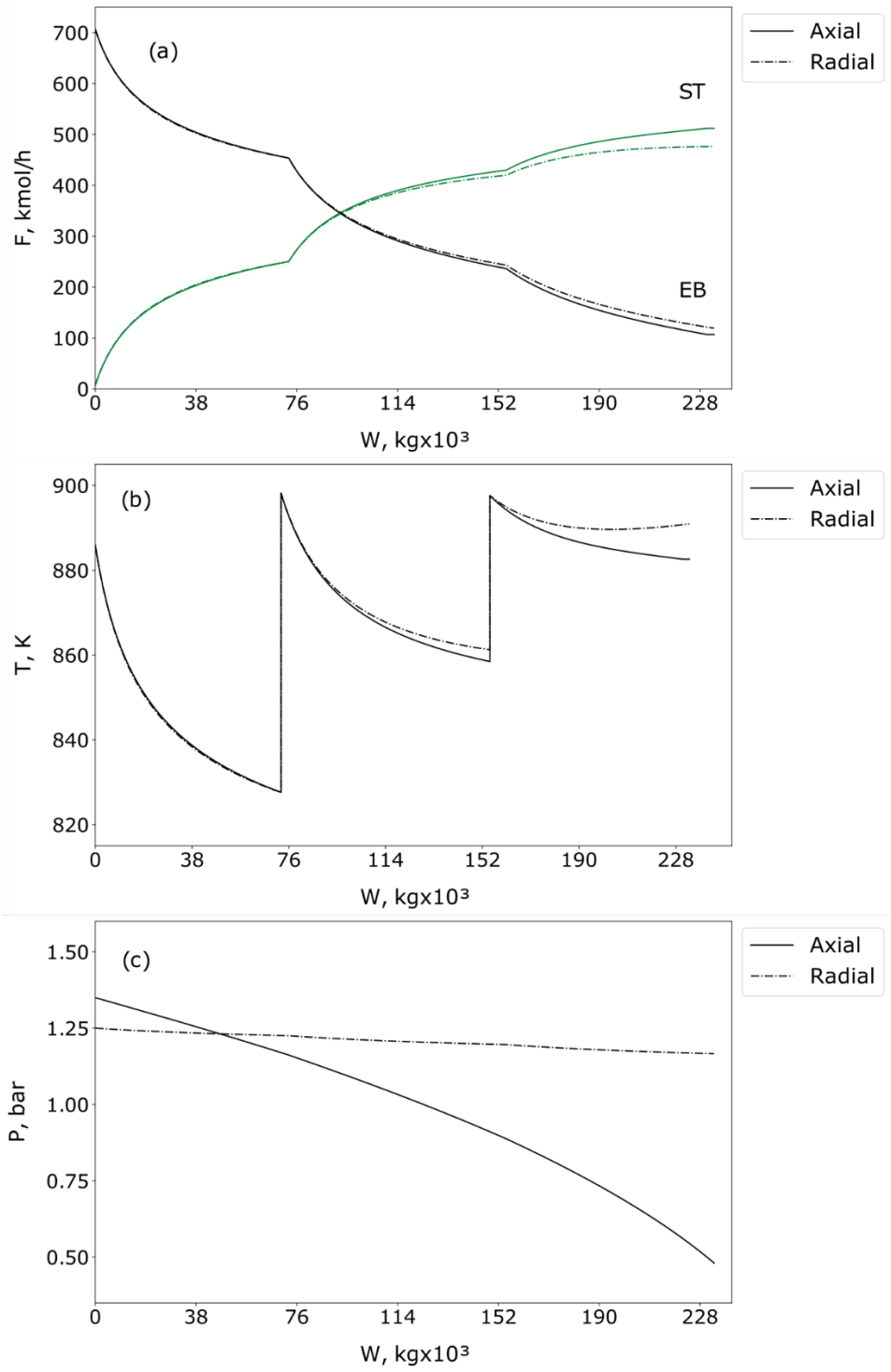

Figure 7 – Results obtained for axial-flow and radial-flow multibed reactors at sub-optimal operating conditions in terms of (a) EB and ST molar flow rates (b) temperature profiles (c) pressure drop.

In terms of ST conversion and selectivity, the axial-flow reactor led to the best results, as, with the corresponding inlet pressures, a substantial part of the process occurs at lower pressures than using the radial-flow configuration. As

observed by Dimian & Bildea (2019) operating at “the lowest workable pressure” significantly increases equilibrium conversion, and the lowest workable pressure limit is defined by outlet pressure. Although performing better in the initial scenario, the inlet pressure of the axial-flow reactor had already been set close to the minimum value to obtain an outlet pressure of 0.5 bar, so there was no possibility to gain either ST selectivity or conversion on the axial-flow reactor by lowering the feed pressure, while this was feasible to the radial-flow reactor.

When analyzing component profiles in Figure 7 (a) and temperature profiles in Figure 7 (b) it is possible to infer that, under the sub-optimal conditions, most of the main reaction took place at the initial part of each bed, and also that the EB consumption occurred mostly in the first bed. As noticed by Dimian & Bildea (2019), the reaction zone with lower reaction rates may provide a catalyst reserve for ensuring flexibility in operation, which is important for working with different feed rates and preventing negative impacts due to catalyst deactivation. However, under these conditions, a small part of the main reaction occurred in the third bed, where the lower pressures favor equilibrium conversion and selectivity. Thus, optimization of the operating conditions can be crucial to define changes in inlet temperatures that can reduce reaction rates in the first bed while an increase in the second and third beds, with gains in conversion and selectivity.

In Figure 7 (b), one can observe that the temperature in the radial-flow reactor increased along the 3rd bed. This was a consequence of exothermic reactions prevailing over endothermic ones. Thus, as ST is produced by an endothermic reaction, it is possible to infer that side reactions were prevailing over the main reaction, therefore ST selectivity was compromised. However, as the pressure drop was considerably low, the radial-flow reactor could operate at lower feed pressures, which would enhance ST selectivity.

5.2. OPTIMIZATION

5.2.1. Gradient-based optimization and design comparison

The Pareto front for each reactor was obtained preserving ρ_b, ε_b, ρ_s, ε_s, inner radius, and molar feed ratios from Table 2, also preserving bed length in case of the radial-flow configuration. Eleven points were obtained for each reactor using weights equally spaced ranging from 0.0 to 1.0. They are presented in Figure 8, except for points with conversion below 55%, which were removed for better visualization. The optimal parameters with respective weights, X_{ST}, and S_{ST} are presented in Table 8 for the axial-flow reactor, and Table 9 for the radial-flow reactor. The optimal results compared to the sub-optimal are presented in Table 10.

The number of internal collocation points used to solve the intraparticle diffusion problem when performing the optimization was set as 3 instead of 6, as used when simulating the multi-bed reactor at predefined conditions. This choice was a consequence of the necessity of long times to perform the optimization, because of long times to evaluate the objective function, which with 3 internal collocation points were about 7 seconds per evaluation, while with 6 internal collocation points were greater than 15 seconds per evaluation (by the time of experiments). The difference between the effectiveness factor values was less than 0.5% and between X_{ST} values was less than 10^{-4} though.

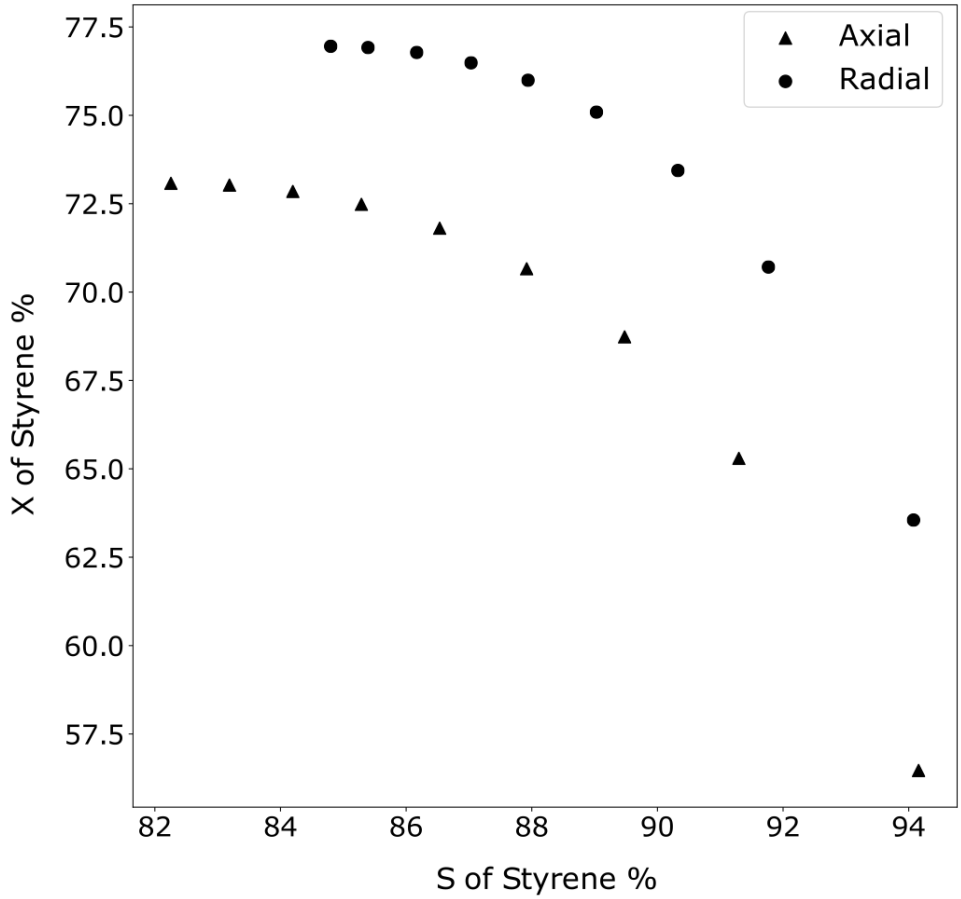

Figure 8 – Pareto front for each reactor configuration with the objective functions of maximizing Styrene conversion and selectivity.

Table 8 – Styrene selectivity and conversion, weights for objective functions, and respective optimal parameters for the axial-flow reactor in the Pareto front.

					T_{in}, K			*W*, kg x 10^3		
w_1	w_2	S_{ST}, %	X_{ST}, %	P_{in}, bar	T_1	T_2	T_3	W_1	W_2	W_3
0	1	82.3	73.1	1.324	876.1	910.8	913.1	74.1	72.5	72.5
0.1	0.9	83.2	73.0	1.319	871.2	907.6	913.2	73.0	72.5	72.5
0.2	0.8	84.2	72.8	1.316	866.4	903.0	913.2	72.9	72.5	72.5
0.3	0.7	85.3	72.5	1.315	861.4	897.1	913.1	74.1	72.5	72.5
0.4	0.6	86.5	71.8	1.309	854.3	890.7	913.2	72.9	72.5	72.5
0.5	0.5	87.9	70.7	1.303	846.2	881.8	913.2	72.9	72.5	72.5
0.6	0.4	89.5	68.7	1.298	835.5	869.9	913.2	73.0	72.6	72.5
0.7	0.3	91.3	65.3	1.289	820.9	853.5	912.2	73.2	72.6	72.5
0.8	0.2	94.2	56.5	1.276	808.4	837.5	892.3	72.8	72.5	72.5
0.9	0.1	97.3	38.0	1.259	800.0	820.0	843.0	72.5	72.5	72.5
1	0	97.4	37.2	1.258	800.0	820.0	840.0	72.5	72.5	72.5

Table 9 – Styrene selectivity and conversion, weights for objective functions, and respective optimal parameters for the radial-flow reactor in the Pareto front.

					T, K			*W*, kg x 10^3		
w_1	w_2	S_{ST}, %	X_{ST}, %	P_{in}, bar	T_1	T_2	T_3	W_1	W_2	W_3
0	1	84.8	77.0	0.669	886.4	913.1	913.2	74.5	72.5	72.5
0.1	0.9	85.4	76.9	0.668	881.1	911.4	913.2	73.0	72.7	72.5
0.2	0.8	86.2	76.8	0.667	874.5	908.3	913.1	73.0	72.7	72.5
0.3	0.7	87.0	76.5	0.666	870.2	902.2	913.1	73.2	72.5	72.5
0.4	0.6	87.9	76.0	0.666	863.8	896.1	913.1	74.0	72.5	72.5
0.5	0.5	89.0	75.1	0.664	855.7	888.2	913.1	73.3	72.7	72.5
0.6	0.4	90.3	73.4	0.663	856.5	869.3	913.1	72.9	72.7	72.5
0.7	0.3	91.8	70.7	0.660	839.4	856.6	913.1	72.8	72.6	72.5
0.8	0.2	94.1	63.6	0.658	818.7	847.4	896.0	75.8	72.5	72.5
0.9	0.1	97.6	40.7	0.650	800.0	820.0	840.0	72.5	72.5	72.5
1	0	97.6	40.7	0.650	800.0	820.0	840.0	72.5	72.5	72.5

Table 10 – Selectivity and conversion for reactors operating at optimal conditions compared to sub-optimal conditions.

		Axial-flow		Radial-flow	
w_1	w_2	ΔS_{ST}, %	ΔX_{ST}, %	ΔS_{ST}, %	ΔX_{ST}, %
0	1	-1.86	1.68	5.00	10.58
0.1	0.9	-0.92	1.63	5.59	10.54
0.2	0.8	0.08	1.45	6.37	10.41
0.3	0.7	1.18	1.08	7.23	10.11
0.4	0.6	2.42	0.41	8.14	9.62
0.5	0.5	3.81	-0.74	9.23	8.72
0.6	0.4	5.37	-2.66	10.52	7.06
0.7	0.3	7.18	-6.10	11.97	4.34
0.8	0.2	10.04	-14.93	14.27	-2.82
0.9	0.1	13.21	-33.40	17.83	-25.71
1	0	13.30	-34.24	17.83	-25.71

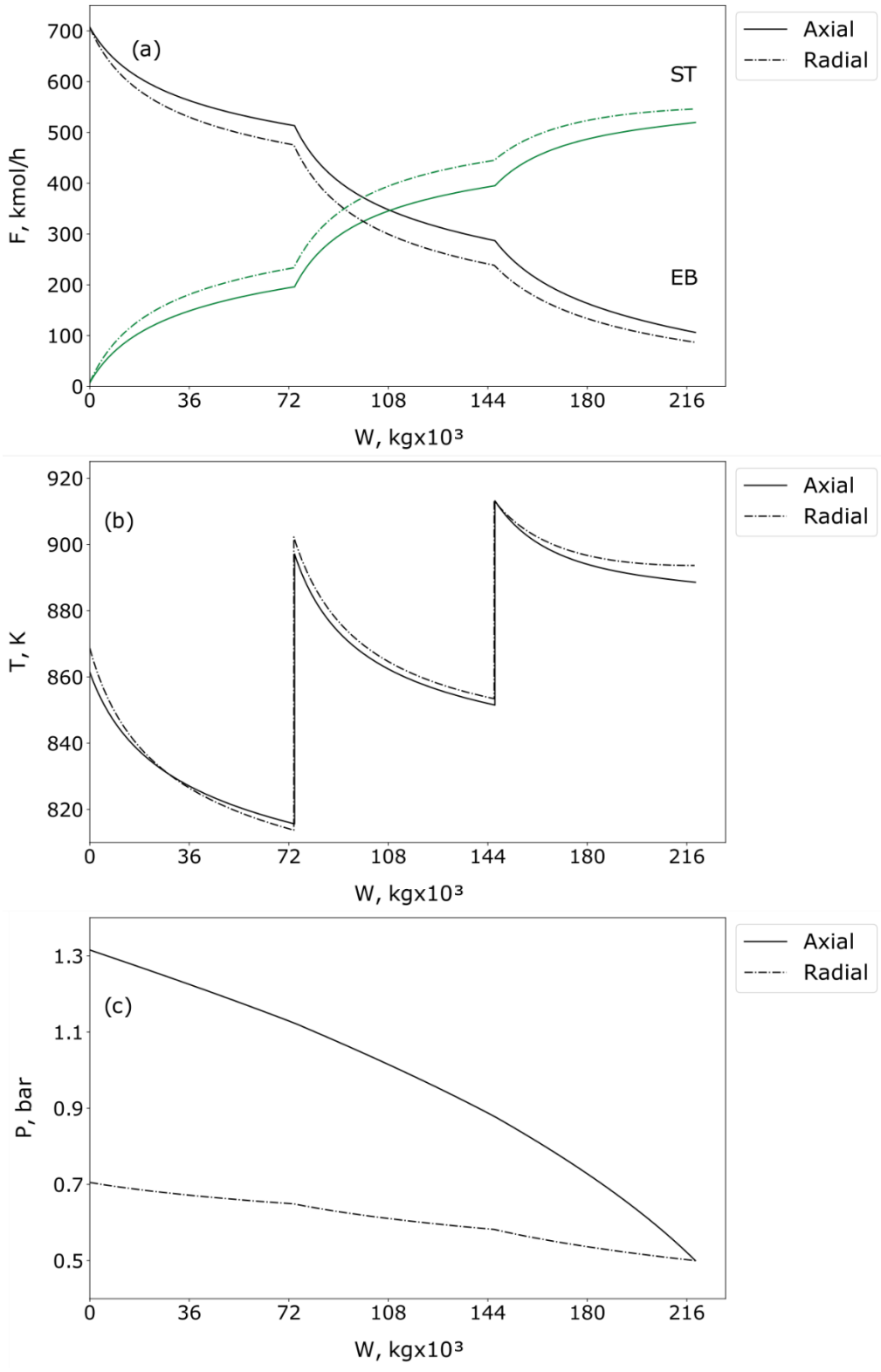

Figure 9 – Results at optimal operating conditions using S_{ST} and X_{ST} weights of respectively 0.7 and 0.3 for axial-flow and radial-flow multibed reactors in terms of (a) EB and ST molar flow rates (b) temperature profiles (c) pressure drop.

By the smooth shape of the Pareto front (Figure 8) it is possible to infer that optimization proceeded well. Previously testing initial guesses and variable boundaries at the pseudo-homogenous reactor was essential to avoid infeasible solutions and local minima. The boundaries defined for inlet pressure performed well in preventing the infeasible solutions but were not active in any of the Pareto solutions (Table 8 and Table 9). This way, these boundaries have worked only as a numerical resource for performing the optimization, and not as limitations to the simulated process.

Comparing the process at optimal operating conditions to itself at sub-optimal, it was possible to verify a great improvement in terms of both S_{ST} and X_{ST} in most points for the radial-flow reactor, while, for the axial-flow reactor, results from weighing selectivity with values lower than 0.2 or greater than 0.4 were worst in terms of either S_{ST} or X_{ST}. This was expected because the pressure, which is an important driver to gain selectivity, had an expressive margin to be reduced at the radial-flow reactor, whereas it had been set at its lower limit for the axial-flow reactor at sub-optimal conditions.

Comparing the two optimized reactor configurations, differently from results obtained at sub-optimal operating conditions, as most of the reactions in the radial-flow reactor occur at lower pressures than in the axial-flow reactor, it produced better results in terms of both S_{ST} and X_{ST}, what is evident in Figure 8 and Figure 9. Therefore, the radial-flow reactor has proved to be a better alternative than the axial-flow for industrial manufacturing.

For both the axial-flow and radial-flow reactors, reducing X_{ST} weights in the range from 1.0 to 0.7 resulted in a significant improvement in S_{ST} compared to the magnitude of loss in X_{ST} conversion. After the weight of 0.5 for X_{ST}, further reductions led to more significant losses in X_{ST} and to smaller improvements in S_{ST}.

Considering the results of the Pareto front (Figure 8, Table 8, and Table 9), weighing S_{ST} and X_{ST} with respectively 0.3 and 0.7 is an adequate solution. In this point, the values S_{ST} and X_{ST} were respectively 85.3% and 72.5% for the axial-flow reactor and 87.0% and 76.5% for the radial-flow reactor, corresponding to increments in S_{ST} and X_{ST} of respectively 1.18% and 1.08% for the axial-flow reactor and 7.23% and 10.11% for the radial-flow reactor when compared to sub-optimal dimensions and operational conditions.

Profiles of F_{EB}, F_{ST}, T, and P for this solution are presented in Figure 9. It is possible to observe, comparing it to Figure 7, that the amount of styrene produced in the second and third beds is greater in the optimized conditions compared to the sub-optimal conditions. It has a positive impact on both X_{ST} and S_{ST} and can be related to changes in the inlet temperature scheme. Under optimized conditions, the inlet temperature of each catalyst bed is greater than that of previous beds, except when upper optimization boundaries were active and they assume the same value. The values of temperatures T_2 and T_3 from the first line of Table 9 are both 913.15K although their values differ in the table due to rounding errors. The optimized inlet temperature scheme can be explained as a strategy for reactions to take place in the second and third beds, in which lower operating pressures lead to gains in selectivity and conversion. Besides, by analyzing the temperature profiles it is possible to notice that endothermic reactions prevail over exothermic all over the reactors, as the temperature profile is decrescent at each bed.

In Table 8 and Table 9, it is possible to notice that, as the weights for S_{ST} versus X_{ST} increase, there is a tendency of operating at lower pressures and lower temperatures. The former is directly related to selectivity, as observed by Lee & Froment (2008). The latter results in lower X_{ST}, thus lower F_{ST}, so increases the rate of the direct reaction of the equilibrium between EB and ST avoiding the side reaction which consumes ST and H_2 to produce TO and CH_4. It is remarkable that although higher temperatures might increase the rate of the main reaction and the equilibrium conversion, for a problem with such boundaries and constraints as defined in this study, the optimal X_{ST} does not occur with the inlet temperature at its upper boundary at the first two catalyst beds for the axial-flow reactor and the first catalyst bed for the radial-flow reactor. This might be also attributed to the significant gain in selectivity as the pressure decreases along the reactors, which makes it favorable that most of the reactions occur at the last beds.

One can observe that catalyst loading in the first bed was greater than in the second and third beds for both reactors (Table 8 and Table 9), except when all lower bounds were active (S_{ST} weights of 0.9 and 1.0). Conversely, catalyst loading in the last bed was smaller than in both the other beds (except when other lower bounds were active). However, it is hard to trace patterns for changes in

W_1 and W_2 as a consequence of changes in S_{ST} and X_{ST} weights. Probably gradients of the weighted objective functions with respect to these variables were negligible in the neighborhood of the solutions. Therefore, it is expected that this design aspect would have its impact on reactor performance better explained by non-gradient-based algorithms. Moreover, in the optimal front, total catalyst loading was less than in suboptimal conditions. This has contributed to lower pressure drop, enabling the reactors to operate with lower inlet pressures.

For the axial-flow reactor, with the constraints defined in this study, when using 0.9 as the weight for S_{ST} most of the boundaries of the variables were active, and when using 1.0 all boundaries were active, except the inlet pressure, although the outlet pressure constraint was active. Thus, results were quite similar in these points. Differently, for the radial-flow reactor, when using 0.9 as the weight for S_{ST} all the boundaries were active, except the inlet pressure, so there was no margin for gain in selectivity, the reason why results in this point are the same as when using 1.0 as the weight for S_{ST}.

5.2.2. Evolutionary algorithm experiments

5.2.2.1. Two objective problems

The corresponding values of objectives and decision variables for the solutions obtained using the complete heterogeneous model are provided in Supplementary Material of the published article (Leite, et al., 2023) rather than in the main body of this dissertation due to the extension of the results. The Pareto fronts obtained for the three-bed configuration using discrete values for steam-to-ethylbenzene molar feed ratios (S-EB) are presented in Figure 10.

The solutions are well distributed on the Pareto fronts, although one might notice that the region of high conversion seems to contain a relatively lower density of solutions. The distribution of solutions suggests that for a given S-EB, increments in conversion to its maximum feasible limit might be undesirable from an engineering perspective because it necessarily leads to significant losses in selectivity. Furthermore, the high conversion region is more sensitive to changes in decision variables. Overestimating the necessary heat supplied to operate in

maximum single-pass conversion leads to losses in both conversion and selectivity, which is evidently undesirable.

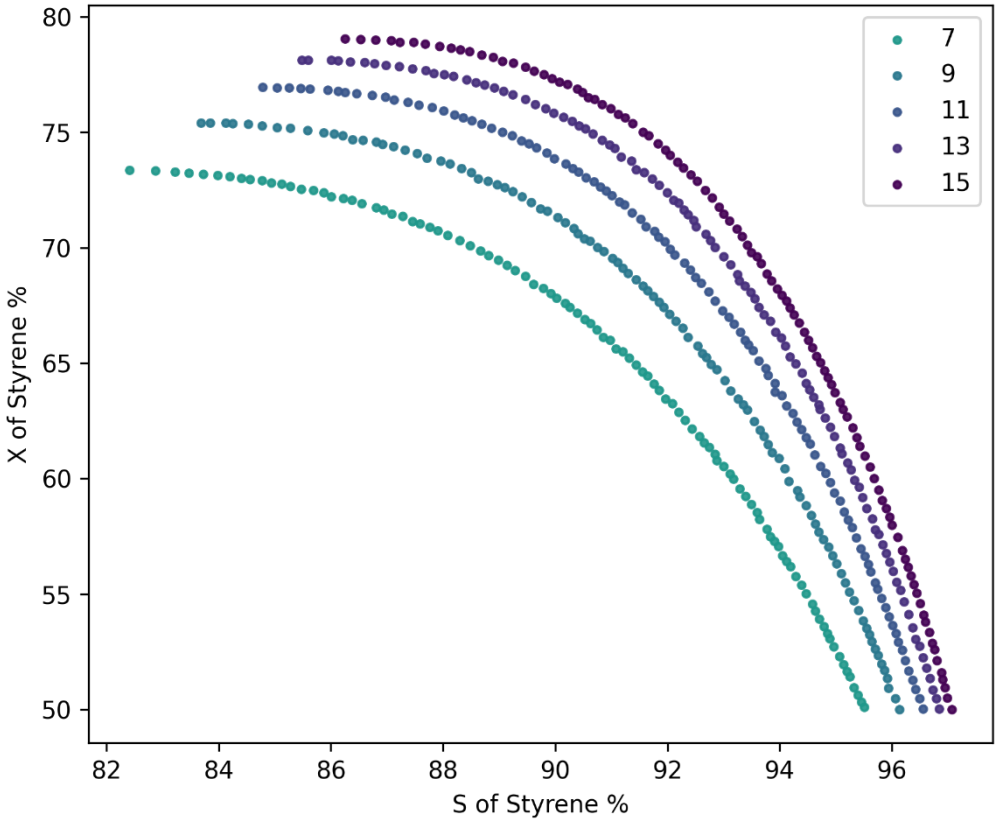

Figure 10 – Pareto fronts obtained for discrete levels of steam-to-ethylbenzene ratio in three-bed reactor configuration.

For an optimized reactor working with a single-pass conversion of 70%, which is usual in industrial practice (ENI-Versalis, s.d.), a reduction from the base case of an S-EB of 11 to 9 would imply a loss of approximately 1.3% in selectivity, and further reduction to 7 would lead to an additional loss of 2.2% (total of 3.5%). Conversely, increments from 11 to 13 and 13 to 15 lead to 0.9% and 0.5% improvements. The benefits of operating with higher S-EB are significantly less pronounced when operating at lower single-pass conversion. For instance, increasing the ratio from 11 to 13 and 13 to 15 at a 50% single-pass conversion led to increments of 0.3% and 0.2% in selectivity. Besides the direct benefits in selectivity when using higher S-EB, in the high conversion region (≥ 70%), it can be beneficial for preventing coke deposition and catalyst deactivation, as this region is operated at higher temperatures.

The molar flow rates, temperature, and pressure profiles for solutions of 70% single-pass conversion for the three-bed reactor are presented in Figure 11. It is possible to notice that, as the S-EB increases, the emphasis on the reaction in the last two catalyst beds becomes more significant. Using the highest steam ratio evaluated, only 20% of total styrene conversion occurred in the first reaction bed. Even with the base S-EB (11), only 26% of total styrene conversion occurred in the first reaction bed. This can be justified as, by lowering the reactants' partial pressures, steam favors the direct main reaction to the extent that the heat supplied in the last two catalyst beds is enough to perform the 70% conversion.

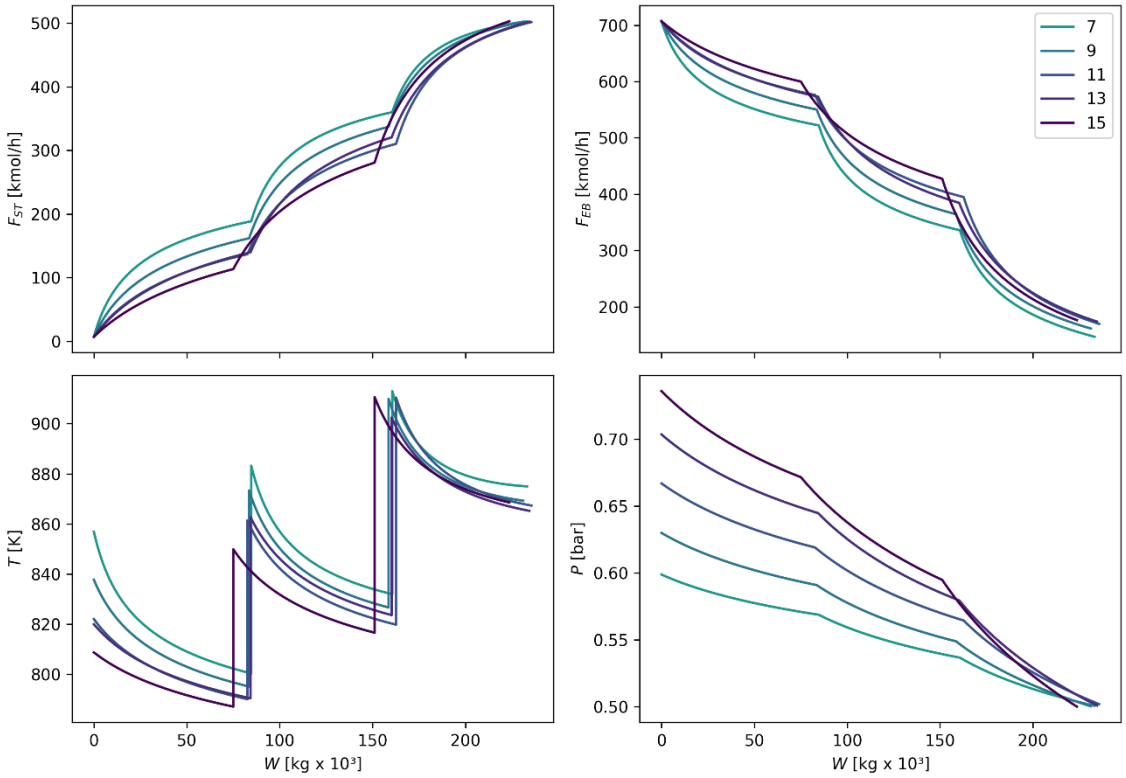

Figure 11 – Molar flow rates, temperature, and pressure profiles for solutions near 70% of single-pass conversion for the three-bed reactor using different steam-to-ethylbenzene feed ratios.

The top-level Parallel coordinates visualizations for the three-bed reactor (top) and two-bed reactor (bottom) are presented in Figure 12. When producing these figures, the decision variables were normalized using their boundaries from Table 5. However, to be comparable in the normalized scale, all temperatures were scaled between 800.00 and 913.15. The objectives were scaled considering

the minima and maxima from the combined populations obtained for each reactor configuration. Their original values are preserved for comparison in Figure 13.

.

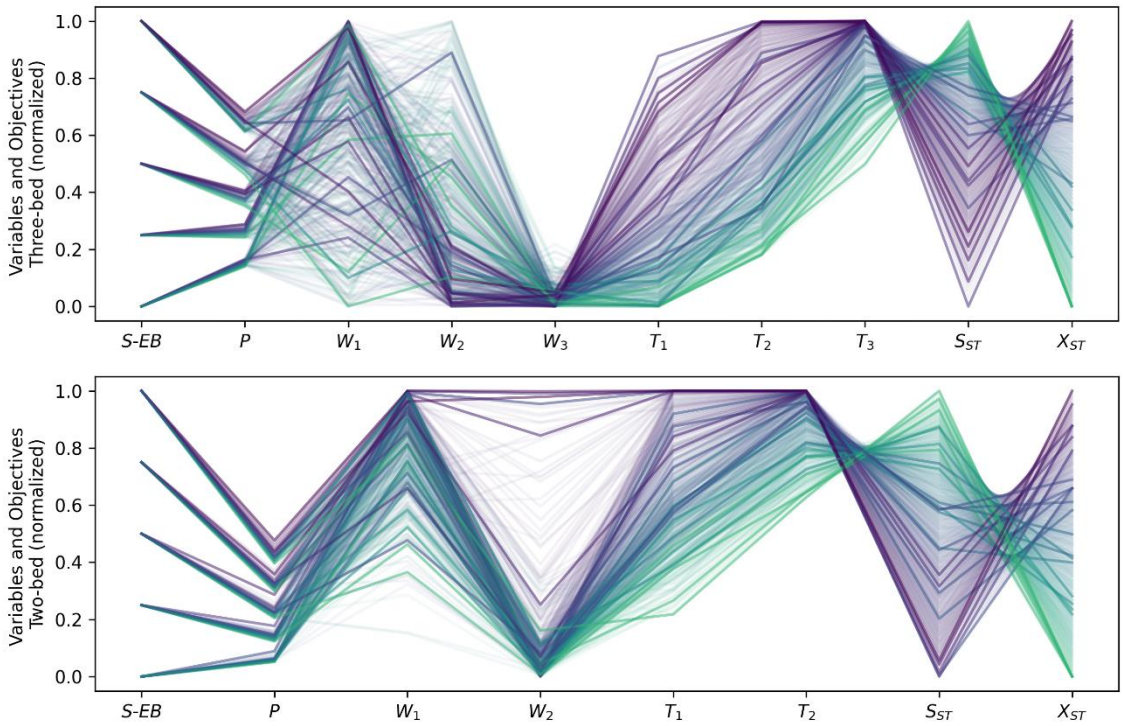

Figure 12 – Parallel coordinates visualization for two-objective problems of three-bed (top) and two-bed reactor (bottom) design. The color scale was defined based on the values of conversion.

When analyzing the Pareto fronts obtained for a two-bed reactor configuration (Figure 13), it is evident that using two catalyst beds leads to limitations in attainable single-pass conversion compared to the three-bed design. In solutions near the maximum attainable conversion, both catalyst beds' upper boundaries for inlet temperatures are active, as observed in Figure 12. Diversely, when the three-bed design is adopted, the first catalyst bed never operates at its temperature upper bound. Thus, the choice for operating inlet temperatures must consider other design aspects and decision variables, even when maximum single-pass conversion is desired. The distribution of the heat supplied to the endothermic reaction should emphasize regions of the reactor operated with the lowest pressure if the design allows. It leads to a distribution in

which the inlet temperature of each catalyst bed is greater than or equal to previous beds (Figure 12), which agrees with our previous results.

In both reactor configurations, the catalyst loading of the first bed is usually biased towards higher values, although this behavior is even emphasized in the two-bed design. Conversely, the catalyst loading of the following beds is biased towards lower values. Notice that for most solutions, the catalyst loading of the last reactor bed is close to its lower bound. The maximum attainable single-pass conversion in the two-bed reactor is an exception, in which the catalyst loadings of both reactors are close to their upper bounds. In this situation, increments in the reactor residence time would still increase its single-pass conversion. Moreover, although random distribution prevails to some extent concerning the catalyst loading of the intermediate bed in the three-bed configuration, especially for high single-pass conversion, some bias towards lower values is observed.

Although the impact of the catalyst loading of initial beds in reactor selectivity and conversion might be relatively small compared to other decision variables, considering the sparsity in the solutions distribution, it might lead to other benefits. In industrial practice, a surplus in catalyst loading might be helpful to ensure flexibility in operation and reduce operational temperatures, which has the advantage of preventing catalyst deactivation and coke deposition, besides slightly reducing heating costs.

In a two-bed design, for S-EB greater than or equal to 11 (Figure 13), the benefits in reactor selectivity provided by an additional catalyst bed are relatively small, considering a single-pass conversion of up to 70%. It endorses the analysis of molar flow rates and temperature profiles in Figure 11, as the operating temperatures of the first reactor bed, for achieving a 70% single-pass conversion, are considerably higher with S-EB lesser than or equal to 9, which favors side reactions. Therefore, the benefits of the third catalyst bed in conversion and selectivity are more significant when working with S-EB lesser than or equal to 9 or when greater single-pass conversion is desired, such as 75%. In the latter, the third bed is not only desirable but necessary considering the EB molar feed rate and residence time adopted. Working with relatively low steam ratios can be especially useful when fuel and furnace costs are relatively high and when heat recovery efficiency in the industrial unit is low. Environmental aspects can also motivate a reduction in fuel consumption in the furnaces. A higher conversion is

especially desired when the plant performance and capacity are limited by separation and recycling units or the reactor's original dimensions. Considering market fluctuations and limitations in other related processes, the flexibility assured by an additional catalyst bed might be important to providing stable economic returns.

Previous studies have already demonstrated that the energy cost for running highly endothermic reactions may be significantly higher than process equipment cost in terms of annualized costs (Dimian & Bildea, 2019). The third catalyst bed should incur additional energy demand due to interstage re-heating, which should be balanced against its benefits in conversion and selectivity, therefore, fresh ethylbenzene and recycling costs. Moreover, it leads to additional equipment and catalyst costs. When fresh ethylbenzene costs prevail, selectivity should be emphasized, as long as separation and recycling units provide the necessary capacity. In this context, a two-bed reactor operating with an intermediate-low (11-9) steam ratio is likely preferred.

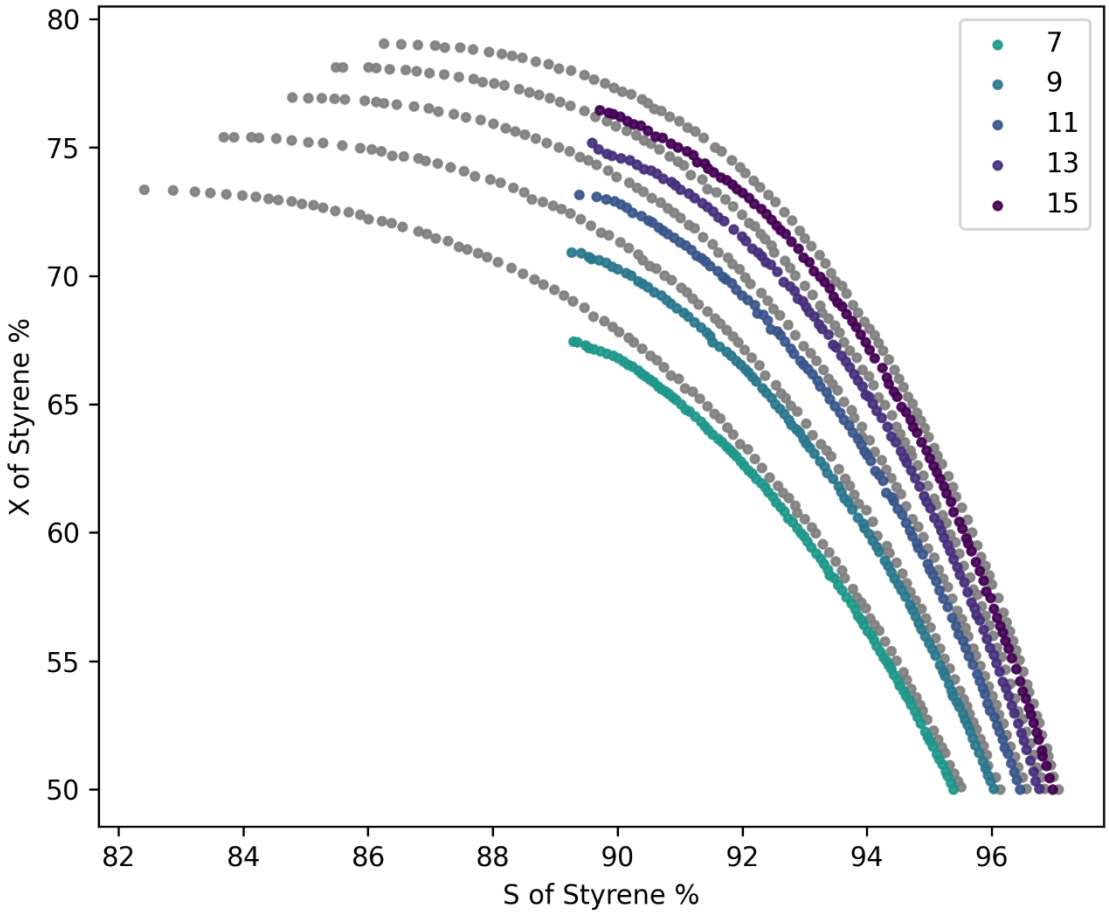

Figure 13 – Pareto fronts obtained for discrete levels of steam-to-ethylbenzene ratio in two-bed reactor configuration (in colors) compared to three-bed configuration (in light grey).

To illustrate the impact of diffusional phenomena on the kinetic model, Figure 14 presents the effectiveness factors of the four reactions along reactor length. Operational conditions and dimensions were defined considering the optimized three-bed reactor operating with S-EB of 11 and 70% of conversion. Notice that, in the inlet section of each catalyst bed, due to interstage (re)heating, the surface reaction rates should be considerably high. Therefore, considering the impact of reaction rates in the intraparticle transport equation (presented in Appendix A), the effectiveness factors of reactions consuming EB are at their lowest levels. Conversely, the fourth reaction presents a different pattern, as it consumes ST and H_2. In this reaction, as the molar fractions of ST and H_2 are greater inside than outside the porous pellets, the effectiveness factors are greater than one. When ST and H_2 molar fractions are significantly small at the

entrance of the reactor, the effectiveness factor of this reaction tends to assume remarkably high values. As for the fourth reaction, the effectiveness factor of the third reaction starts with very high values because the molar fraction of one of its reactants (H_2) is considerably low in the reactor inlet.

When operating the reactor beds with inlet temperatures in ascending order, the partial pressure gradients of components are less pronounced than if the operating temperatures had been in descending order or even. It occurs because the reactants' partial pressures are higher close to the reactor inlet, leading to higher reaction rates at the pellets' surface, increasing composition gradients. Although probably in a minimal magnitude, the catalyst deactivation might be reduced for a given single pass conversion if operating the reactors at the optimized inlet temperature scheme based on conversion and selectivity.

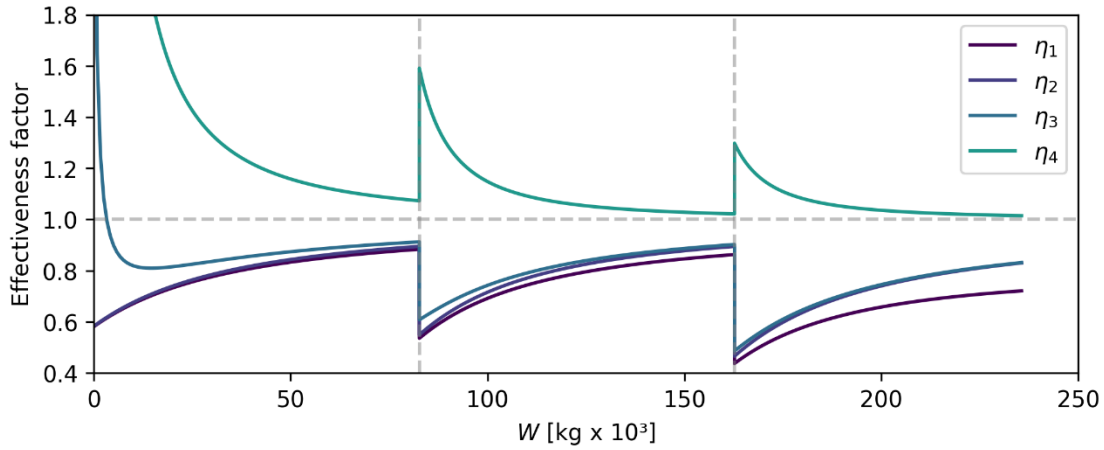

Figure 14 – Profiles of effectiveness factors along optimized three-bed reactor operating with 70% single-pass conversion and a steam-to-ethylbenzene feed ratio of 11.

5.2.2.2. Three objective problems

The two-dimensional perspective of the Pareto front obtained for the three-objective problem using GDE3 is presented in Figure 15. The three-dimensional perspectives for solutions obtained by GDE3 and NSDE-R are presented in Figure 16 and Figure 17. The *M*-NN crowding metric has effectively produced well-distributed solutions in the objective space, with no bias towards preferred reference directions. This strategy can be advantageous when the natural distribution of elements in the front differs from the usual reference directions of

multi and many-objective problems. The maximum level of the third objective (minimizing S-EB) does not correspond to a single best solution in the other two objectives but a set of non-dominated solutions. Therefore, using the *M*-NN survival, the distribution of elements in the front is more homogeneous on different levels of S-EB than using reference directions.

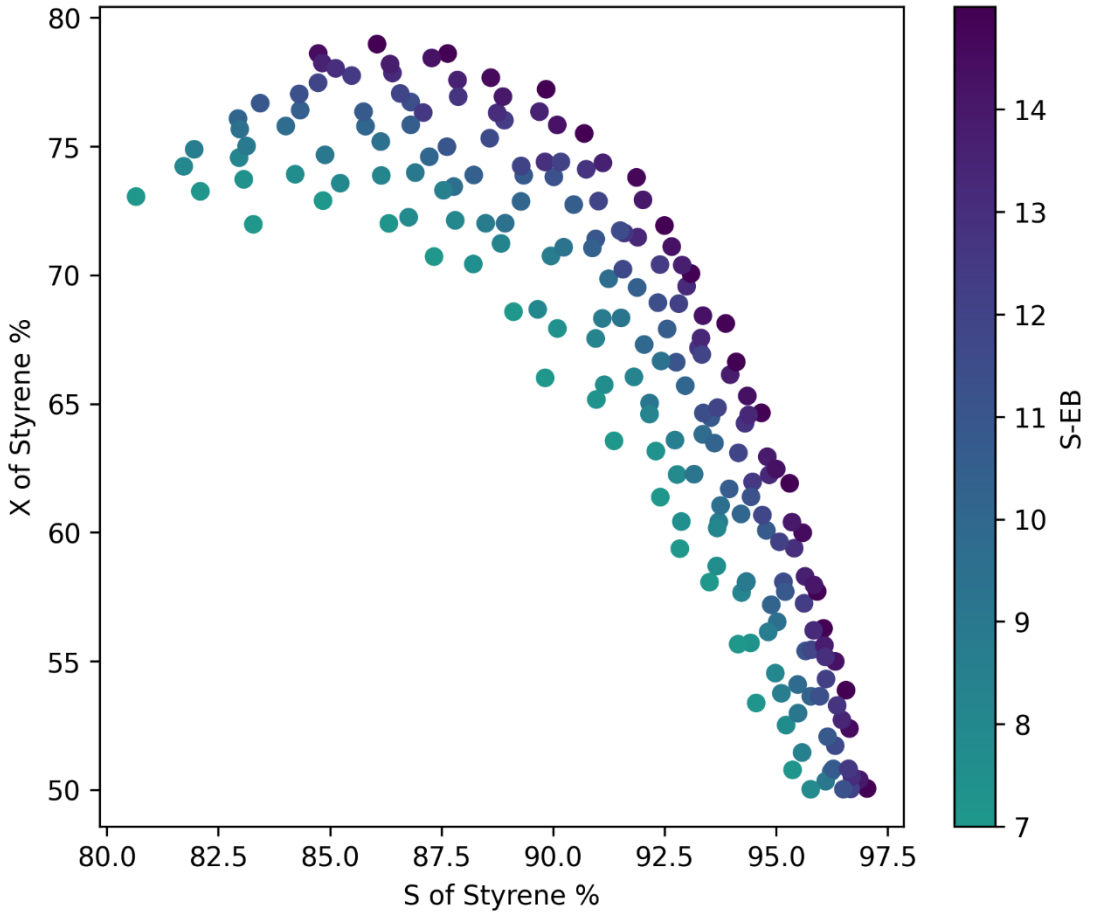

Figure 15 – Two-dimensional perspective of the Pareto optimal solutions obtained by GDE3 in the three-objective problem.

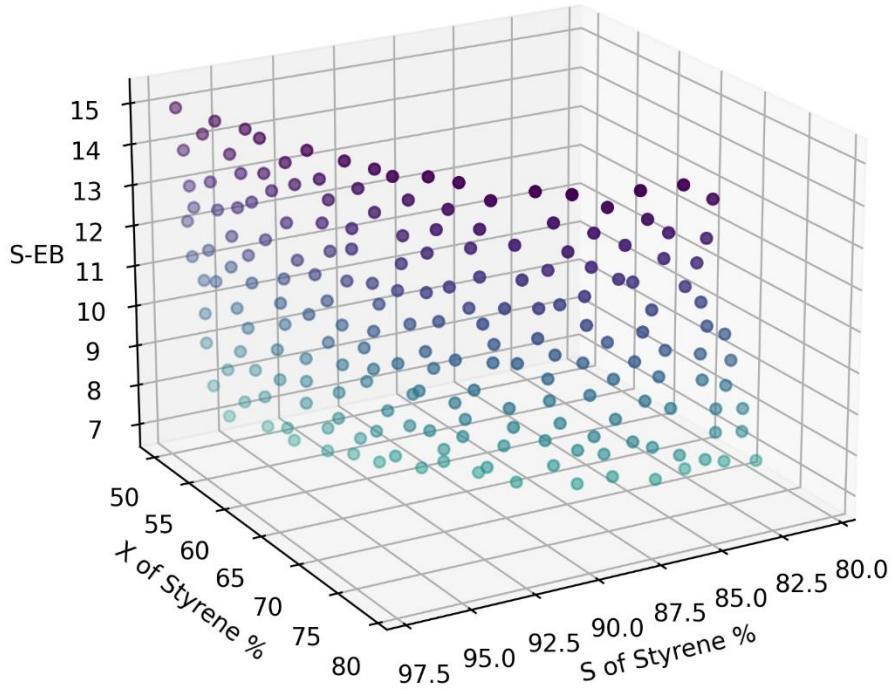

Figure 16 – Three-dimensional perspective of the Pareto optimal solutions obtained by GDE3 in the three-objective problem.

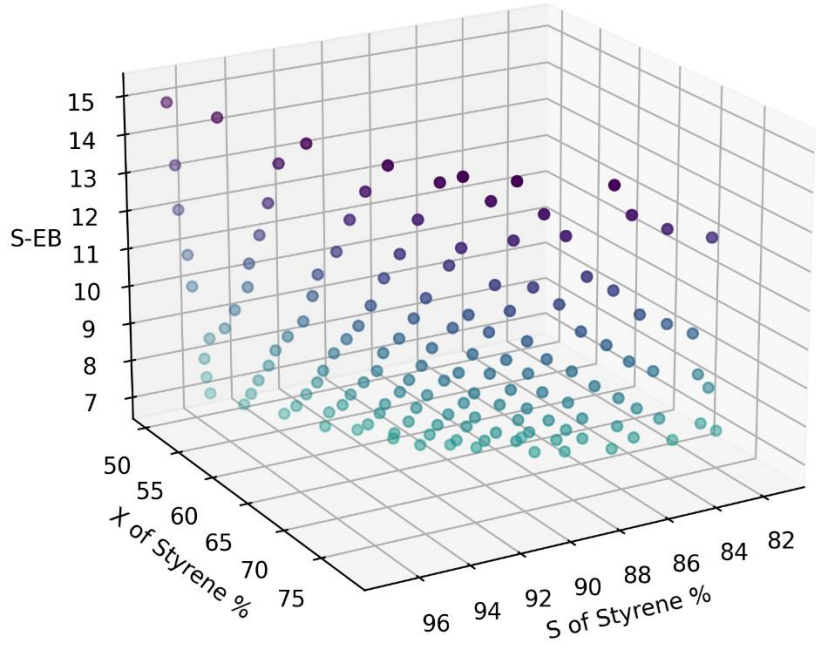

Figure 17 – Three-dimensional perspective of the Pareto optimal solutions obtained by NSDE-R in the three-objective problem.

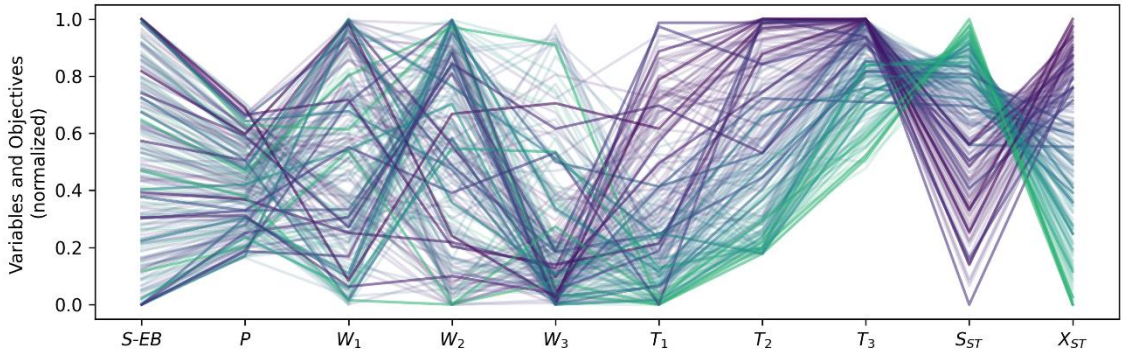

Figure 18 – Parallel coordinates visualization for the three-objective problem.

The Parallel coordinates visualization for the results obtained using GDE3-MNN is presented in Figure 18. The same normalization for the two-objective problem was performed. Although some general behavior is preserved, differences in results are evident when compared to Figure 12. As expected, the inlet temperatures are greater for solutions with more emphasis on conversion than selectivity. However, random factors in the heat distribution are considerably more pronounced when evaluated from the three-objective perspective. As previously observed, the heat supplied should emphasize reactor regions operated with the lowest pressure. Although most solutions still preserve the inlet temperatures in ascending order from the first to the last catalyst bed, in 41 of the 200, the temperature of a subsequent bed was greater than the previous one. The author and his colleague could not trace any pattern to justify this behavior based on fundamental aspects considering either catalyst loading or steam ratio. Therefore, it is likely that the reduced selective pressure due to the greater sparsity in objective space has produced solutions that could still be improved in all objectives simultaneously. The greater sparsity of solutions is noticeable when comparing Figure 15 to Figure 10, considering the distances between one solution and its closest neighbors considering selectivity and conversion. This adversity is expected to be reduced if the population size is increased, which would, conversely, increase computational costs.

Concerning the catalyst loading of each reactor bed, the preferred values previously observed in the two-objective results are no longer observed for neither the first nor the second beds. In the third, some bias towards lower values is preserved, although the occurrence of solutions with higher values is

remarkable. As a general pattern, there is a negative correlation between the catalyst loading of the first and the second beds. Therefore, the algorithm has converged to solutions that, to some extent, preserve optimal residence times.

In this sense, when pursuing a deep conceptual analysis of the impact of decision variables on reactor performance, the two-objective approach might be a better choice, although a more sophisticated three-objective strategy can be adopted. It is essential to formulate the problem and choose the corresponding algorithm according to the purpose of the investigation, which, in the current study, was better addressed by a more straightforward strategy. The three-objective approach still has the advantage of producing continuous results over S-EB that can be further used in integrated decision-making processes.

Different regions in the decision space were explored, diversely from the previous results obtained using exact methods, because of the stochastic nature of the algorithms herein adopted. In industrial practice, the flexibility of choosing between different scenarios of comparable performance might prevail over the precision of exact methods.

6. CONCLUSIONS

Styrene is one of the most used industrial monomers as it is a major component of many polymer-based products. Modeling, simulating, and optimizing styrene reactor design and operation is critical to improving plant performance and economic returns. The objectives of the current work consisted of simulating and optimizing styrene reactor design and operation exploiting particular aspects of different optimization strategies. The simulations performed were consistent and the programming structure has proved versatile to simulate different scenarios.

Under baseline conditions, previously adopted in the literature, the axial-flow reactor produced better results than radial-flow, but the former had a lower margin of improvement after optimization, due to the outlet pressure already being set at the minimum possible. Comparing the two optimized reactor configurations, as most of the reactions in the radial-flow reactor occurred at lower pressures than in the axial-flow reactor, it produced better results in terms of both S_{ST} and X_{ST}. Therefore, considering the same limitation for outlet pressure, the radial-flow reactor has proved to be a better alternative than axial-flow for industrial manufacturing. Improvements because of optimization in the radial-flow reactor were more significant than in the axial-flow, because of the great impact of reducing the operating pressure. Gains were observed in both reactors due to optimized inlet temperature schemes, that favor reactions to take place in the final catalyst beds, in which pressures are lower than in initial beds. Under optimized conditions, the inlet temperature of each catalyst bed is greater than that of previous beds, except when optimization upper boundaries were active.

The steam-to-ethylbenzene molar feed ratio, a relevant heat consumer in the process, had its impact on conversion and selectivity investigated using two-objective and three-objective evolutionary approaches. The benefits of high steam ratios in the reactor selectivity are more relevant when operating at relatively high single-pass conversion (70%), in which improvements in selectivity are more emphasized than in low conversion operation. A high conversion is especially desired when the plant performance and capacity are limited by separation and recycling units or the reactor's original dimensions. A three-bed

reactor configuration is beneficial for operating at high single-pass conversion and low steam-to-ethylbenzene feed ratios (≤ 9), besides ensuring flexibility to absorb market fluctuations and limitations in related processes.

A bias towards adopting relatively higher catalyst loading in the first reactor bed was observed in both two- and three-bed reactor designs. Although its impact on selectivity and conversion might be small, it leads to other benefits, such as preventing catalyst deactivation, reducing heating costs, and assuring more flexibility in operation. Furthermore, this study reinforces the importance of low pressure to reactor performance. Because of pressure drop, the inlet temperature of each catalyst bed should be greater than previous ones, except when limited by upper bounds, as a mechanism to favor reactions to occur in regions with lower pressures.

An additional contribution of the current work is the reproducibility of results as python packages for orthogonal collocation (Leite, 2022b), differential evolution (Leite, 2022a), and styrene reactor model (Leite, 2022c) are publicly available.

7. DATA AVAILABILITY

The code implemented throughout this study is available in three public repositories listed below:

- pymoode: https://github.com/mooscaliaproject/pymoode
- collocation: https://github.com/bruscalia/collocation
- styrene: https://github.com/bruscalia/styrene

Any of these can be incorporated into a Python 3 environment by the following command line:

pip install -e git+<URL>#egg=<NAME_OF_PACKAGE>

Also, the user might clone the git repository or download its code on a zip file and then run setup.py install.

The package pymoode is also available on PyPi and can be directly installed:

pip install pymoode

Complete tutorials are available in each repository.

REFERENCES

Abbass, H. A., Sarker, R. & Newton, C., 2001. PDE: a Pareto-frontier differential evolution approach for multi-objective optimization problems. *Proceedings of the 2001 congress on evolutionary computation (IEEE Cat. No. 01TH8546),* Volume 2, pp. 971-978.

Abdalla, B., Elnashaie, S., Alkhowaiter, S. & Elshishini, S., 1994. Intrinsic kinetics and industrial reactors modelling for the dehydrogenation of ethylbenzene to styrene on promoted iron oxide catalysts. *Applied Catalysis A: General,* 113(1), pp. 89-102.

Ali, E. & Hadj-Kali, M., 2018. Energy efficiency analysis of styrene production by adiabatic ethylbenzene dehydrogenation using exergy analysis and heat integration. *Polish Journal of Chemical Technology,* 20(1), pp. 35-46.

Ayaz, M., Panwar, A. & Pant, M., 2020. A Brief Review on Multi-objective Differential Evolution. In: M. Pant, et al. eds. *Soft Computing: Theories and Applications. Advances in Intelligent Systems and Computing.* Singapore: Springer, pp. 1027-1040.

Babu, B. V. & Anbarasu, B., 2005. *Multi-objective differential evolution (MODE): an evolutionary algorithm for multi-objective optimization problems (MOOPs).* s.l., Proceedings of international symposium and 58th annual session of IIChE.

Babu, B. V., Chakole, P. G. & Mubeen, J. H. S., 2005. Multiobjective differential evolution (MODE) for optimization of adiabatic styrene reactor. *Chem. Eng. Sci.,* Volume 60, pp. 4822-4837.

Bakhshi Ani, A., Ale Ebrahim, H. & Azarhoosh, M. J., 2015. Simulation and multi-objective optimization of a trickle-bed reactor for diesel hydrotreating by a heterogeneous model using non-dominated sorting genetic algorithm II. *Energy Fuels,* 29(5), pp. 3041-3051.

Beck, J., Friedrich, D., Brandani, S. & Fraga, E. S., 2015. Multi-objective optimisation using surrogate models for the design of VPSA systems. *Comput. Chem. Eng.,* Volume 82, pp. 318-329.

Blank, J. & Deb, K., 2020. pymoo: Multi-Objective Optimization in Python. *IEEE Access,* Volume 8, pp. 89497-89509.

Boggs, P. T. & Tolle, J. W., 1996. Sequential Quadratic Programming. *Acta Numerica,* Volume 4, pp. 1-51.

Business Wire, 2021. *The Global Styrene Market - Forecast to 2023.* [Online] Available at: https://www.businesswire.com/news/home/20181126005427/en/The-Global-Styrene-Market---Forecast-to-2023-Expected-to-Register-a-CAGR-of-2---ResearchAndMarkets.com
[Accessed 20 October 2021].

Campos, B. L. O., Costa, A. O. S. C., Figueiredo, K. C. S. & Costa, E. F., 2018. Performance comparison of different mathematical models in the simulation of a solar desalination by humidification-dehumidification. *Desalination,* Volume 437, pp. 184-194.

Carra, S. & Forni, L., 1965. Kinetics of Catalytic Dehydrogenation of Ethylbenzene to Styrene. *Industrial and Engineering Chemistry Process Design and Development,* July, 4(3), pp. 281-285.

Chaudhari, P. & Garg, S., 2019. Multi-objective optimization of maleic anhydride circulating fluidized bed (CFB) reactors. *Chem. Eng. Res. Des.,* Volume 141, pp. 115-132.

Chaudhari, P. et al., 2022. Comparison of NSGA-III with NSGA-II for multi objective optimization of adiabatic styrene reactor. *Materials Today: Proceedings,* 57(4), pp. 1509-1514.

Cheng, J., Yen, G. G. & Zhang, G., 2016. A grid-based adaptive multi-objective differential evolution algorithm. *Inform. Sci.,* Volume 367-368, pp. 890-908.

Chen, S., 2006. Styrene. In: *Kirk-Othmer Encyclopedia of Chemical Technology.* s.l.:s.n.

Chevron Phillips Chemical, 2021. *Styrene.* [Online] Available at: https://www.cpchem.com/what-we-do/solutions/aromatics/products/styrene [Accessed 20 October 2021].

Coello, C. A. C., Lamont, G. B. & Van Veldhuizen, D. A., 2007. *Evolutionary algorithms for solving multi-objective problems.* 2nd ed. New York: Springer.

Costa, E., Lage, P. & Biscaia, E., 2003. On the numerical solution and optimization of styrene polymerization in tubular reactors. *Computers & Chemical Engineering,* 27(11), pp. 1591-1604.

Deb, K., 2001. *Multi-Objective Optimization Using Evolutionary Algorithms.* 1st ed. Chichester: John Wiley & Sons.

Deb, K., 2004. Introduction to Genetic Algorithms for Engineering Optimization. In: G. C. Onwubolu & B. V. Babu, eds. *New Optimization Techniques in Engineering Studies in Fuzziness and Soft Computing, vol 141.* Heidelberg: Springer Verlag Berlin Heidelberg, pp. 13-51.

Deb, K. & Jain, H., 2014. An evolutionary many-objective optimization algorithm using reference-point-based nondominated sorting approach, part I: solving problems with box constraints. *IEEE Transactions on Evolutionary Computation,* 18(4), pp. 577-601.

Deb, K., Pratap, A., Agarwal, S. & Meyarivan, T. A. M. T., 2002. A Fast and Elitist Multiobjective Genetic Algorithm: NSGA-II. *IEEE transactions on evolutionary computation,* 6(2), pp. 182-197.

Devoldere, K. & Froment, G., 1999. Coke Formation and Gasification in the Catalytic Dehydrogenation. *Industrial & Engineering Chemistry Research,* 38(7), pp. 2626-2633.

Dimian, A. C. & Bildea, C. S., 2019. Energy Efficient Styrene Process: Design and Plantwide Control. *Ind. Eng. Chem. Res.,* 58(12), pp. 4890-4905.

Dimian, A. C., Bildea, C. S. & Kiss, A. A., 2019. *Applications in Design and Simulation of Sustainable Chemical Processes.* s.l.:Elsevier.

Elnashaie, S. S. E. H. & Elshishini, S. S., 1993. *Modelling Simulation and Otimization of Industrial Fixed Bed Catalytic Reactors.* Yverdon: Gordon and Breach Science Publishers.

ENI-Versalis, n.d. *Licensing: Styrenics, proprietary process technology.* [Online] Available at: www.versalis.eni.com [Accessed 23 October 2021].

Ergun, S., 1952. Fluid Flow through Packed Columns. *Chemical Engineering Progress,* 48(2), pp. 89-94.

Fairbanks, D. F. & Wilke, C. R., 1950. Diffusion Coefficients in Multicomponent Gas Mixtures. *Industrial & Engineering Chemistry,* 42(3), pp. 471-475.

Fan, Q. & Yan, X., 2018. Multi-objective modified differential evolution algorithm with archive-base mutation for solving multi-objective p-xylene oxidation process. *J Intell Manuf,* Volume 29, pp. 35-49.

Fedotov, A. S. et al., 2021. Production of styrene by dehydrogenation of ethylbenzene on a [Re, W]/γ-Al2O3 (K, Ce)/α-Al2O3 porous ceramic catalytic converter. *Chem. Eng. Process. - Process Intensifi.,* Volume 160, p. 108265.

Fierens, S. K. et al., 2015. Exploring the Full Potential of Reversible Deactivation Radical Polymerization Using Pareto-Optimal Fronts. *Polymers,* 7(4), pp. 655-679.

Finlayson, B. A., 1973. Orthogonal Collocation in Chemical Reaction Engineering. *Catalysis Reviews,* 10(1), pp. 69-138.

Focus on Surfactants, 2020. LyondellBasell and Sinopec announce JV to manufacture propylene oxide and styrene monomer in China. *Focus on Surfactants,* 2020(3), p. 2.

Fogler, H. S., 1999. *Elements Of Chemical Reaction Engineering.* 3rd ed. Upper Saddle River(N.J.): Prentice Hall PTR.

Froment, G. F. & Bischoff, K. B., 1979. *Chemical Reactor Analysis and Design.* 1st ed. New York(N.Y.): John Wiley and Sons.

Fuller, E. N., Schettler, P. D. & Giddings, J., 1966. A new method for prediction of binary gas-phase diffusion coefficients. *Industrial and Engineering Chemistry,* 58(5), pp. 18-27.

Gujarathi, A. M. & Babu, B. V., 2010. Multi-objective optimization of industrial styrene reactor: Adiabatic and pseudo-isothermal operation. *Chem. Eng. Sci.,* Volume 65, pp. 2009-2026.

Hicks, R. E., 1970. Pressure Drop in Packed Beds of Spheres. *Industrial & Engineering Chemistry Fundamentals,* 9(3), pp. 500-502.

Iorio, A. W. & Li, X., 2004. Solving rotated multi-objective optimization problems using differential evolution. In: G. Webb & X. Yu, eds. *Australasian joint conference on artificial intelligence.* Heidelberg: Springer-Verlag Berlin Heidelberg, pp. 861-872.

Ishibuchi, H., Imada, R., Setoguchi, Y. & Nojima, Y., 2018. How to Specify a Reference Point in Hypervolume Calculation for Fair Performance Comparison. *Evol. Comput.,* 26(3), pp. 411-440.

Jain, H. & Deb, K., 2014. An evolutionary many-objective optimization algorithm using reference-point based nondominated sorting approach, part II: handling constraints and extending to an adaptive approach. *IEEE Transactions on Evolutionary Computation,* 18(4), pp. 602-622.

James, D. & Castor, W., 2011. Styrene. In: *Ullmann's Encyclopedia of Industrial Chemistry.* s.l.:s.n.

Jones, E., Oliphant, T., Peterson, P. & others, 2001-. *SciPy: Open Source Scientific Tools for Python.* s.l.:s.n.

Kraft, D., 1988. *A Software for Sequential Quadratic Programming.* s.l.:Wiss. Berichtswesen d. DFVLR.

Kukkonen, S., 2007. Performance assessment of Generalized Differential Evolution 3 (GDE3) with a given set of problems. *2007 IEEE Congress on Evolutionary Computation,* 1(1), pp. 3593-3600.

Kukkonen, S. & Deb, K., 2006a. *Improved Pruning of Non-Dominated Solutions Based on Crowding Distance for Bi-Objective Optimization Problems.* Vancouver, s.n., pp. 1179-1186.

Kukkonen, S. & Deb, K., 2006b. A fast and effective method for pruning of non-dominated solutions in many-objective problems. In: *Parallel problem solving from nature-PPSN IX.* Berlin: Springer, pp. 553-562.

Kukkonen, S. & Lampinen, J., 2005. GDE3: The third evolution step of generalized differential evolution. *2005 IEEE congress on evolutionary computation,* Volume 1, pp. 443-450.

Lee, W. J., 2005. *Ethylbenzene Dehydrogenation into Styrene: Kinetic Modeling and Reactor Simulation,* College Station, Texas: Texas A&M University.

Lee, W. J. & Froment, G. F., 2008. Ethylbenzene Dehydrogenation into Styrene: Kinetic Modeling and Reactor Simulation. *Ind. Eng. Chem. Res.,* 47(23), pp. 9183-9194.

Leite, B., 2022b. *A Python module to solve boundary value problems using orthogonal collocation.* [Online] Available at: https://github.com/bruscalia/collocation [Accessed 30 10 2022].

Leite, B., Costa, A. O. S. & Costa Junior, E. F., 2021. Simulation and optimization of axial-flow and radial-flow reactors for dehydrogenation of ethylbenzene into styrene based on a heterogeneous kinetic model. *Chem. Eng. Sci.,* Volume 244, p. 116805.

Leite, B., Costa, A. O. S. & Costa Junior, E. F., 2023. Multi-objective optimization of adiabatic styrene reactors using Generalized Differential Evolution 3 (GDE3). *Chem. Eng. Sci.,* Volume 265, p. 118196.

Leite, B. S. C. F., 2022a. *pymoode: Differential Evolution in Python.* [Online] Available at: https://github.com/mooscaliaproject/pymoode [Accessed 06 June 2022].

Leite, B. S. C. F., 2022b. *collocation.* [Online] Available at: https://github.com/bruscalia/collocation [Accessed 05 June 2022].

Leite, B. S. C. F., 2022c. *styrene.* [Online] Available at: https://github.com/bruscalia/styrene [Accessed 1 December 2022].

Li, J. C., 2007. Radial-Flow Packed-Bed Reactors. In: *Ullmann's Encyclopedia of Industrial Chemistry.* s.l.:s.n.

Li, Y., Xu, J., Yu, W. & Ray, A. K., 2020. Multi-objective optimization of sequential simulated moving bed for the purification of xylo-oligosaccharides. *Chem. Eng. Sci.,* Volume 211, p. 115279.

Luenberger, D. G. & Ye, Y., 2008. *Linear and Nonlinear Programming.* 3rd ed. Stanford: Springer.

Luyben, W. L., 2011. Design and Control of the Styrene Process. *Industrial & Engineering Chemistry Research,* 50(3), p. 1231–1246.

McKetta Jr, J., 1993. *Chemical Processing Handbook.* Boca Raton: CRC Press.

Meima, G. R. & Menon, P. G., 2001. Catalyst deactivation phenomena in styrene production. *Applied Catalysis A: General,* 212(1-2), pp. 239-245.

Nocedal, J. & Wright, S. J., 2006. *Numerical Optimization.* 2nd ed. New York: Springer.

Önal, I., Yalçin, N., Uygun, E. & Öztürk, H., 1990. Simulation and optimization of three existing ethylbenzene dehydrogenation reactors in series. *Mathematical and Computer Modelling,* Volume 14, pp. 263-267.

Price, K. V., Storn, R. M. & Lampinen, J. A., 2005. *Differential Evolution: A Practical Approach to Global Optimization.* 1st ed. Springer: Berlin.

Rangaiah, G. P., Feng, Zemin, Z. & Hoadley, A. F., 2020. Multi-Objective Optimization Applications in Chemical Process Engineering: Tutorial and Review. *Processes,* 8(5), p. 508.

Rangaiah, G. P. & Sharma, S., 2017. *Differential Evolution in Chemical Engineering: Developments and Applications.* s.l.:World Scientific.

Rase, H. F., 2000. *Handbook of Commercial Catalysts: Heterogeneous Catalysts.* Boca Raton(FL): CRC Press.

Reddy, P. S., Rani, K. Y. & Patwardhan, S. C., 2017. Multi-objective optimization of a reactive batch distillation process using reduced order model. *Comput. Chem. Eng.,* Volume 106, pp. 40-56.

Reddy, S. R. & Dulikravich, G. S., 2019. Many-objective differential evolution optimization based on reference points: NSDE-R. *Struct. Multidisc. Optim.,* Volume 60, pp. 1455-1473.

Reid, R. C., Prausnitz, J. M. & Poling, B. E., 1987. *The Properties of Gases and Liquids.* 4th ed. New York: McGraw-Hill.

Robič, T. & Filipič, B., 2005. DEMO: Differential Evolution for Multiobjective Optimization. In: C. Coello Coello, A. Hernández Aguirre & E. Zitzler, eds. *Evolutionary Multi-Criterion Optimization. EMO 2005. Lecture Notes in Computer Science.* Heidelberg: Springer, Berlin, pp. 520-533.

Sancheti, S. V. & Yadav, G. D., 2021. Highly selective production of styrene by non-oxidative dehydrogenation of ethylbenzene over molybdenum-zirconium mixed oxide catalyst in fixed bed reactor: Activity, stability and kinetics. *Catal. Commun.,* Volume 154, p. 106307.

Sandler, S. I., 1999. Chapter 3: Conservation of Energy. In: *Chemical, biochemical, and engineering thermodynamics.* 3rd ed. Hoboken(N.J.): John Wiley, pp. 47-98.

Sharma, S. & Rangaiah, G. P., 2013. An improved multi-objective differential evolution with a termination criterion for optimizing chemical processes. *Comput. Chem. Eng.,* Volume 56, pp. 155-173.

Sheel, J. G. P. & Crowe, C. M., 1969. Simulation and optimization of an existing ethylbenzene dehydrogenation reactor. *The Canadian Journal of Chemical Engineering,* 47(2), pp. 183-187.

Sheppard, C., Maler, E. & Caram, H., 1986. Ethylbenzene dehydrogenation reactor model. *Industrial and Engineering Chemistry Process Design and Development,* 25(1), pp. 207-210.

Snyder, J. D. & Subramaniam, B., 1994. A novel reverse flow strategy for ethylbenzene dehydrogenation in a packed-bed reactor. *Chemical Engineering Science,* 49(24), pp. 5585-5601.

Srinivas, N. & Deb, K., 1994. Muiltiobjective Optimization Using Nondominated Sorting in Genetic Algorithms. *Evolutionary Computation,* 2(3), pp. 221-248.

Storn, R. & Price, K., 1997. Differential evolution–a simple and efficient heuristic for global optimization over continuous spaces. *J. Glob. Optim.,* 11(4), pp. 341-359.

Sundaram, K., Sardina, H., Fernandez-Baujin, J. & Hildreth, J., 1991. Styrene plant simulation and optimization. *Hydrocarbon Process.,* 70(1), pp. 93-97.

Tarafder, A., Rangaiah, G. & Ray, A. K., 2005. Multiobjective optimization of an industrial styrene monomer manufacturing process. *Chem. Eng. Sci.,* 60(2), pp. 347-363.

Trivedi, V. & Ramteke, M., 2021. Using following heroes operation in multi-objective differential evolution for fast convergence. *Appl. Soft Comput.,* Volume 104, p. 107225.

Villadsen, J. & Stewart, W. E., 1967. Solution of boundary-value problems by orthogonal collocation. *Chem. Eng. Sci.,* 22(11), pp. 1483-1501.

Wang, G. et al., 2021. Ethylbenzene dehydrogenation over Fe2O3 promoted TiO2-ZrO2 catalysts and corresponding conceptual fluidized bed process. *J. Taiwan Inst. Chem. Eng.,* Volume 120, pp. 1-8.

Xue, F., Sanderson, A. C. & Graves, R. J., 2003. Pareto-based multi-objective differential evolution. *The 2003 Congress on Evolutionary Computation, 2003. CEC'03,* Volume 2, pp. 862-869.

Yee, A. K., Ray, A. K. & Rangaiah, G., 2003. Multiobjective optimization of an industrial styrene reactor. *Comput. Chem. Eng.,* 27(1), pp. 111-130.

Yi, W., Chen, Y., Pei, Z. & Lu, J., 2022. Adaptive differential evolution with ensembling operators for continuous optimization problems. *Swarm Evol. Comput.,* Volume 69, p. 100994.

Zaharie, D., 2009. Influence of crossover on the behavior of Differential Evolution Algorithms. *Appl. Soft Comput.,* 9(3), pp. 1126-1138.

Zhang, Q. & Li, H., 2007. MOEA/D: A multiobjective evolutionary algorithm based on decomposition. *IEEE Trans. Evol. Comput.,* 11(6), pp. 712-731.

Zhang, X., Jin, L., Cui, C. & Sun, J., 2021. A self-adaptive multi-objective dynamic differential evolution algorithm and its application in chemical engineering. *Appl. Soft Comput.,* Volume 106, p. 107317.

Zitzler, E., Laumanns, M. & Thiele, L., 2001. *SPEA2: Improving the strength Pareto evolutionary algorithm.* s.l.:TIK-report.

APPENDIX A

The viscosity of the gas mixture μ was calculated by using the method of Wilke, described by Equations A1 and A2 (Reid, et al., 1987).

$$\mu = \sum_i \frac{y_i \mu_i}{\sum_j y_j \phi_{ij}} \tag{A1}$$

$$\phi_{ij} = \frac{\left[1 + \left(\mu_i / \mu_j\right)^{1/2} \left(M_{m_j} / M_{m_i}\right)^{1/4}\right]^2}{\left[8\left(1 + M_{m_i} / M_{m_j}\right)\right]^{1/2}} \tag{A2}$$

In which y_i is the molar fraction of component i in the gas mixture, μ_i its viscosity, and M_{mi} its molar weight.

For EB, ST, CH_4, BZ, TO and C_2H_4 μ was obtained by the corresponding-states method by Thodos described by Equations A3 and A4 (Lee, 2005).

$$\mu\xi = 4.610 {T_R}^{0.618} - 2.04 e^{-0.449 T_R} + 1.94 e^{-4.058 T_R} + 0.1 \tag{A3}$$

$$\xi = {T_c}^{1/6} {M_m}^{-1/2} {P_c}^{-2/3} \tag{A4}$$

In which, μ is in μP, T_R is the reduced temperature, T_c is the critical temperature in K, P_c is the critical pressure in bar, and ξ is the reduced inverse viscosity in μP^{-1}.

For H_2 and H_2O, μ in μP was obtained by Chapman-Enskog Equation A5 A5 (Reid, et al., 1987).

$$\mu = 26.69 \frac{\sqrt{M_m T}}{\sigma^2 \Omega_v} \tag{A5}$$

For H_2, Ω_v corresponded to Ω_v *(Lennard-Jones)* (Equation A6), while for H_2O it corresponded to Ω_v *(Stockmayer)* (Equation A7).

$$\Omega_v = \frac{A}{T^{*B}} + Ce^{-DT^*} + Ee^{-FT^*} \quad \text{(A6)}$$

$$\Omega_v(Stockmayer) = \Omega_v(Lennard-Jones) + 0.2\,{\delta^2}/{T^*} \quad \text{(A7)}$$

Where $T^* = (k/\varepsilon)\cdot T$, A = 1.16145, B = 0.14874, C = 0.52487, D = 0.77320, E = 2.16178, F = 2.43787. For H_2O δ = 1.

Values of M_m, T_c, P_c, σ, and ε/k were obtained from Reid, et al. (1987).

APPENDIX B

The molecular diffusion coefficient for each component *j* in the multicomponent gas mixture, D_{jm}, was obtained by Equation B1 (Fairbanks & Wilke, 1950).

$$D_{jm} = \frac{1 - y_j}{\sum_{k \neq j} \frac{y_k}{D_{jk}}} \tag{B1}$$

In which D_{jk} is the binary molecular diffusion coefficient for component *j* in component *k*.

The binary molecular diffusion coefficients D_{jk} in m²/s were obtained using Equation B2 (Fuller, et al., 1966).

$$D_{jk} = \frac{10^{-9} T^{1.75}}{P\left[(\sum v)_j^{1/3} + (\sum v)_k^{1/3}\right]^2} \left(\frac{1}{M_{mj}} + \frac{1}{M_{mk}}\right)^{1/2} \tag{B2}$$

And the effective diffusion of each component *j* was obtained by Equation B3 (Froment & Bischoff, 1979).

$$D_{e,j} = \frac{\varepsilon_s}{\tau} D_{jk} \tag{B3}$$

In which τ is the tortuosity factor of the catalyst particle.

APPENDIX C

In the main body of this dissertation, industrial styrene reactors were optimized using the multi-objective algorithm Generalized Differential Evolution 3 (GDE3) to maximize their conversion and selectivity. The discussion was directed towards the fundamental analysis of the results from a chemical engineering perspective, although several optimization aspects of the problem have been investigated. This section will present experiments to evaluate control parameters and compare algorithms to provide a complementary analysis for our main text.

The impact of DE control parameters on GDE3 performance was investigated, and it had its performance compared to the peer algorithm NSGA-II. The comparison between GDE3 and NSGA-II in the two-objective reactor problem aims to evaluate how the DE and GA reproduction operators perform in this problem, considering the two algorithms implemented share the same initialization and survival operators besides the same termination criterion. Although in a previous study Chaudhari et al. (2022) compared the performances of NSGA-III to NSGA-II in a variation of the styrene problem, the problem considered in their study had three objectives, and the main difference between the two algorithms considered was in the survival strategy, which differs substantially from the comparison of the current study. Notice that the pruning method of NSGA-II provides good diversity in the case of two objectives, but when the number of objectives is more than two, the obtained diversity declines drastically (Kukkonen & Deb, 2006b).

When comparing the performances of different algorithms and hyperparameter values in a specific problem, one is limited to the extent of possible inferences regarding general aspects. To general inference, one should perform several experiments on benchmark test problems, which is beyond the scope of the current paper. However, considering future studies on this process and its similarity in modeling aspects with other chemical processes, comparing algorithms and hyperparameters can provide relevant insight to researchers and practitioners. Emphasis on other catalytic processes and plug-flow reactor design from the related chemical processes.

NSGA-II was implemented using the Python *pymoo* library (Blank & Deb, 2020), and GDE3 was implemented as an independent algorithm using *pymoo's*

basic structure. During this study, the *pymoo* version was 0.5.0. The implementation of GDE is available in the Python package *pymoode* (Leite, 2022a).

The optimization problem considered maximizing selectivity and conversion of a three-bed reactor with a fixed S-EB of 11. The impacts of crossover and elitism in parent selection were studied for GDE3, and its performance was compared to NSGA-II. The F parameter was defined in the range [0, 1] in all experiments, randomized by uniform distribution dither. The modified parent selection based on nondominated sorting ranks (Zhang, et al., 2021) was compared to pure DE/rand. It was denoted DE/ranked as distinguished from conventional DE/rand and marked by the RMO (Ranked Mutation Operator) suffix when presenting results. For all two-objective problems, the modified removal strategy in survival by Kukkonen & Deb (2006a) was adopted. When implementing NSGA-II, it was used simulated binary crossover with η = 15 and polynomial mutation with probability = 1/N and η = 20.

A population size of 70 was adopted as it presented adequate convergence in preliminary experiments, and optimization was terminated within 100 generations. The number of generations was determined to be sufficiently large so that, when comparing algorithms, initial higher convergence rates would not possibly hide some difficulty in reaching a true Pareto front and spreading solutions over it in late generations. Experiments were run with 30 different random initialization seeds, a number selected as sufficient to analyze a possible random bias and not too large to be prohibitive due to the computational cost inherent to the problem. The algorithms were compared by the following metrics/criteria:

1. Hypervolume: This metric evaluates the closeness of solutions to an unknown true front and diversity in a combined sense. It calculates the volume (in the objective space) covered by members of a set. It is defined as the union of hypercubes obtained using a reference point and each solution as diagonal corners (Deb, 2001).
2. Convergence speed: It was evaluated by graphical analysis of the hypervolume versus the number of generations.

3. Set Coverage: This metric is denoted as $C(A, B)$. It calculates the proportion of solutions in B, which are weakly dominated by solutions of A (Deb, 2001), and is defined in the range of [0, 1].

Since there is no analytical solution to the two-objective styrene problem, the definition and sampling of elements in the True front might be biased and imprecise. In such a scenario, the usual *IGD* and *GD* metrics for evaluating performance cannot be applied. Alternatively, the hypervolume metric can be calculated for a set of solutions if properly defining a reference point, even though the true front is unknown. A general guideline for the reference point specification is to use a slightly worse point than the nadir point so that the reference point is dominated by all Pareto optimal solutions (i.e., so that all Pareto optimal solutions in a solution set have positive hypervolume contributions) (Ishibuchi, et al., 2018). This hypervolume metric is not free from arbitrary scaling of objectives. Therefore, as suggested by Deb (2001) it was evaluated using normalized objective function values.

When calculating the hypervolumes for comparing different choices of *CR* and different algorithms, the solutions obtained for each choice or algorithm in each independent run were combined and ranked using non-dominated sorting. In each comparison, the reference point for hypervolume calculations was the nadir point of the combined Pareto-optimal solutions added 10^{-6}. Moreover, the nadir and ideal points of the combined Pareto-optimal solutions were used for normalizing both objectives in hypervolume calculations.

In the two-objective problem, both objective functions are nonseparable due to the complex phenomena involved and the interdependence of decision variables in reactor output. Therefore, algorithms with more rotational invariance were expected to present superior performance. It can be done using high CR values in DE algorithms, which fosters mutation and, therefore, preferred search directions. Experiments run with different values for the *CR* parameter are presented in Figure C1. The choice of 0.9 for the *CR* value presented superior performance with statistical significance. Therefore, it was our choice in subsequent experiments on this paper. When comparing performance by completion using *CR* values of 0.9 and 0.7, the Wilcoxon test returned a *p*-value of 0.04.

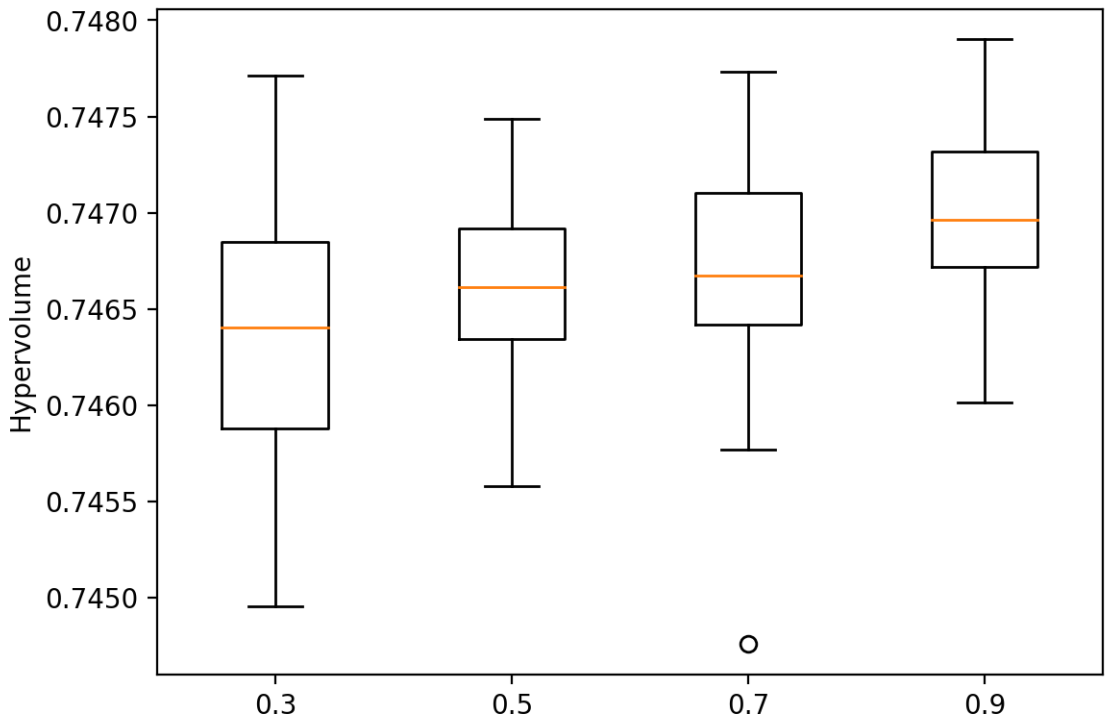

Figure C1 – Distributions of final hypervolume on several independent runs for each value of *CR*.

In the initial generations, as the distribution of elements in the decision space is randomized, the preferred search directions of the problem are not yet evidenced in the decision space. Therefore, the advantages of DE do not yet occur. However, as the solutions converge to the Pareto front, the relative positions of individuals guide DE mutation; thus, GDE3 outperforms NSGA-II, as observed in Figure C2. This superior performance is preserved until algorithm completion as the hypervolumes obtained by GDE3 are significantly greater than those obtained by NSGA-II The Wilcoxon test when comparing GDE3 (DE/rand) to NSGA-II returned a *p*-value of 4×10^{-6}. The comparison is presented in Figure C3.

In this problem, the convergence speed might be improved by adopting the elitism in parent selection proposed by Zhang et al. (2021), herein marked by the RMO suffix. Although improving convergence speed in initial generations, the proposed elitism has not worsened global performance, as it produced similar results to the usual DE/rand by completion. When comparing hypervolumes obtained using GDE3 with DE/rand to DE/ranked (GDE3-RMO) mutation operators, the Wilcoxon test returned a *p*-value of 0.3.

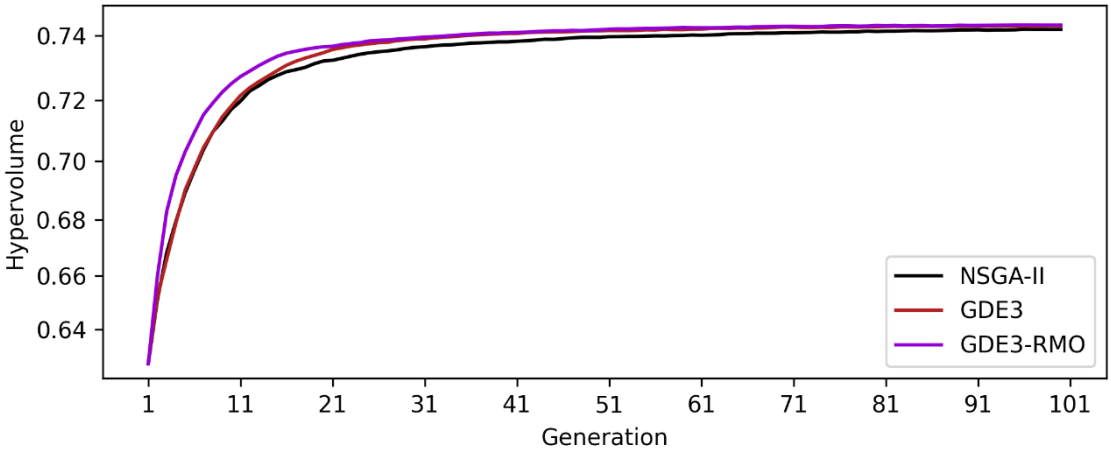

Figure C2 – Median of hypervolume versus the number of generations for each algorithm.

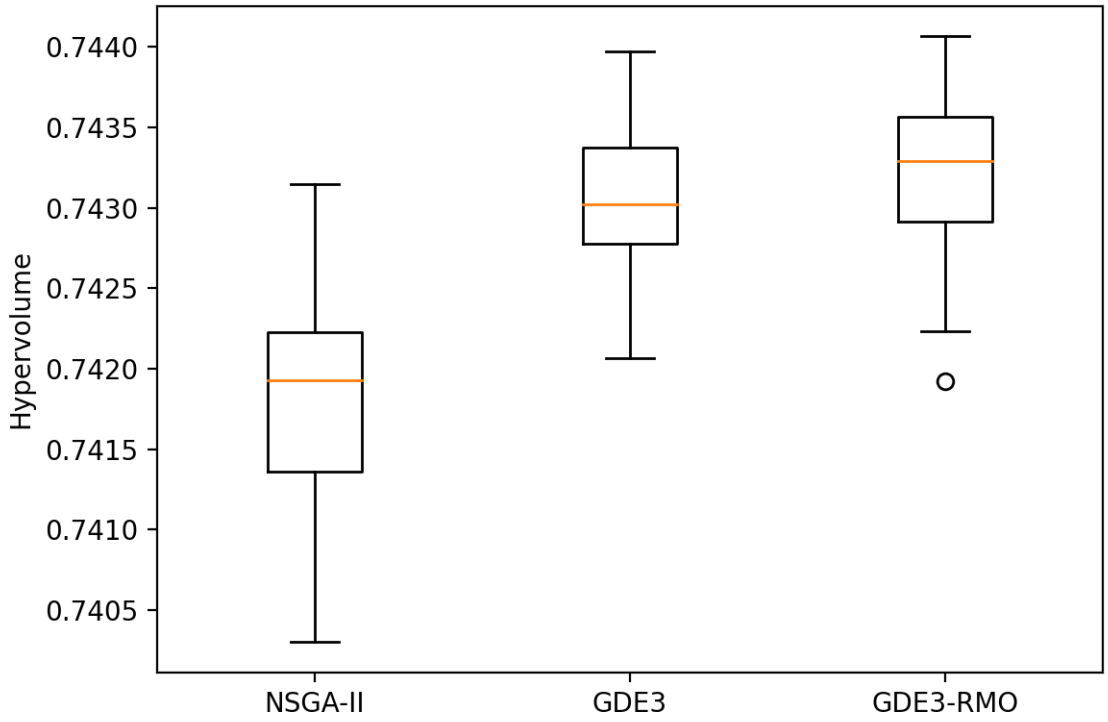

Figure C3 – Distributions of final hypervolume on several independent runs for each algorithm.

The average set coverage pairwise metrics are presented in Table C1. It is possible to notice that an expressive proportion of solutions obtained using NSGA-II are dominated by both the GDE3 variants. Conversely, the proportion of GDE3 solutions dominated by NSGA-II is significantly smaller. It reinforces the superior performance of the DE operator over genetic algorithm reproduction

operators (simulated binary crossover and polynomial mutation) for this problem. Nevertheless, applying NSGA-II to this or a similar problem can also produce valuable results for decision-making and fundamental analysis.

Table C1 – Average set coverage pairwise in the styrene reactor problem.

Algorithms		Average Set Coverage	
A	B	*C*(A, B)	*C*(B, A)
NSGA-II	GDE3	0.083	0.206
NSGA-II	GDE3-RMO	0.078	0.226
GDE3	GDE3-RMO	0.110	0.127

The spacing metric (Deb, 2001) has been evaluated for all three algorithms and produced statistically similar results, likely to be a consequence of using the same survival strategy. The comparison between GDE3 and GDE3-RMO is useful for reinforcing that elitism in parent selection did not worsen the diversity of solutions by completion. The Wilcoxon test for comparing the spacing metrics obtained by each DE variant returned a *p*-value of 0.6. However, to adopt a conservative approach and preserve the diversity of solutions for a deep conceptual analysis of the problem, it was decided to use GDE3 with the usual DE/rand strategy in the heterogeneous reactor model.